High-intensity single-mode laser theory*

Jehuda Ziegler† and Paul R. Berman
Physics Department, New York University, 4 Washington Place, New York, New York 10003
(Received 6 January 1977)

A high-intensity single-mode gas laser is analyzed by several mathematical methods. Exact numerical results are best obtained by solving for the coefficients of a Fourier series solution by using a backward recurrence scheme or a successive convergents method for evaluating a continued fraction. Numerical integration techniques can also be used to convert the periodic boundary conditions to initial conditions and then solve the resulting initial-value problem. Direct analytic integration leads to exact solutions in terms of Bessel functions for the special case of zero detuning, equal decay rates, and neglecting of collision broadening. For general single-mode operation, an improved analytic approximation [the second recursion relation approximation (2RCRA)] is obtained by taking an additional term in the recursion relations for the Fourier coefficients. This approximation predicts the existence of one of the secondary resonances in graphs of the spatially averaged population inversion and quadrature polarization coefficient densities and matches the exact solution from the position of the first resonance and outward independent of the intensity. The 2RCRA also matches the exact detuning curve except at small detunings. The first-order ("rate equation") approximation, by comparison, does not predict any secondary resonances and does not match the exact solution at higher intensities. A physical interpretation for the appearance of the secondary resonances is presented in terms of multiphoton interactions and a prediction for the positions of the resonances for the special case discussed above is obtained. As predicted by Greenstein the exact detuning curves show quantitatively that the Lamb dip decreases and disappears as the intensity increases for high excitations.

I. INTRODUCTION

One of the most successful theories of the laser, which also provides a basic understanding of the interaction between matter and radiation, was presented by Lamb[1] in 1964. In this semiclassical theory, classical electromagnetic fields are assumed to interact with quantum-mechanical atoms, inducing a polarization which in turn supports the field. Self-consistency arguments lead to equations which determine the amplitude and frequency of the field as functions of the induced polarization. A quantum-mechanical analysis of the interaction produces a set of coupled differential equations describing a velocity ensemble averaged density matrix. This density matrix determines the transition-level populations and the polarization. The polarization can then be used to obtain the field amplitude and frequency.

Lamb's perturbation solution explains most of the features of laser operation including the dependence of output intensity on cavity tuning for a single-mode laser (e.g., Lamb dip) and mode competition effects (e.g., mode locking) for the multimode laser. The drawback is that it is only valid for very small field intensities near threshold. Thus for understanding practical laser operation more exact solutions are necessary.

One attempt at such a solution has involved a rate equation or "hole-burning" approximation[1,2] (REA) in which temporal and spatial variations (pulsations) in the population inversion density have been neglected. For the single-mode laser this provides much useful information[3,4] (including the characteristic "hole" or depletion resonance in the population inversion density for atoms whose Doppler-shifted frequency matches the cavity frequency) and is valid at higher intensities than the perturbation solution. However, for the multimode laser it cannot describe mode competition phenomena because it neglects temporal variations.

A theory valid at high intensities has been developed for the single-mode laser by several authors.[5-7] Their method consisted of substituting a spatial Fourier series for the density matrix elements and solving the recursion relations for the coefficients by continued fractions. The results have shown that at high intensities additional resonances appear in graphs of the spatially averaged population inversion density superimposed on the major "hole-burned" depletion resonance. Kuroda and Ogura[8] have proven the convergence of the continued fraction for arbitrary intensities, and the problem of roundoff errors in the numerical evaluation of the continued fraction has been eliminated by using the method of successive convergents.[9]

The Fourier series method has also been used to develop theories for the high-intensity single-mode ring laser,[10] multimode unidirectional traveling-wave laser,[11] and saturated absorption spectroscopy.[9,12,13] For the multimode standing-wave laser this method leads to a multiple (spatial and temporal) Fourier series, and a multiple

continued fraction, which have not been evaluated. Thus the multimode standing-wave laser has still not been treated in a high-intensity formulation.

The purpose of this research has been to develop new methods and improve and expand on the previous methods for solving the high-intensity single-mode laser problem. New physical interpretations for the results, which contribute to the understanding of the laser processes, are also presented. It is to be expected that the additional methods and physical insight will also contribute to related research areas including high-intensity multimode standing-wave laser theory and saturated absorption spectroscopy.

Section II contains a discussion of the physical system and formulates the laser equations as a matrix differential equation with a periodic coefficient matrix. The methods which are used to solve this equation subject to periodic boundary conditions are discussed in Sec. III and presented in Secs. IV–VIII. For a special case of single-mode operation, i.e., when the cavity is tuned to the atomic frequency, the transition-level decay rate are equal, and we neglect collision broadening, an analytic solution is obtained in Secs. IV and V. This case has previously been solved[6,14–16] by various methods and the present research serves to relate these methods and expand upon them. One of the results obtained also allows for the prediction of the secondary resonance positions in graphs of the population inversion density (and polarization) as functions of atomic velocity. Section VI presents an integral equation solution for general single-mode operation which is similar to the integral equation representation of Mathieu functions. In addition, a method for solving the differential equation directly through numerical methods is discussed in Sec. VII. Although this method is not the best for obtaining solutions for the general single-mode laser it should prove useful in other applications, such as the multimode standing-wave laser, which have still not been solved. Section VIII presents a new backward recurrence scheme for evaluating the coefficients in a Fourier series solution. This method and the successive convergents evaluation of the continued fraction provide the best means for obtaining numerical results. Also by truncating the Fourier series and solving for the coefficients analytically we obtain analytic approximations to the solution. In Sec. IX the numerical results are presented and comparisons are made to the analytic approximations. It is shown that the second-order (recursion relation) approximation (2RCRA) is greatly superior to the first-order (rate-equation) approximation (REA). As discussed in the physical interpretation of the results (Sec. X), the second-order approximation includes some of the dynamic coupling between the traveling waves which compose the standing wave whereas the REA treats them as separate waves.

Finally in Sec. XI we discuss the relationship between the relative excitation, field intensity, and cavity tuning. Numerical results are presented and compared to the analytic approximations. A more detailed discussion of this research including listings of the computer programs which obtain the numerical results can be found in Ref. 17.

II. PHYSICAL SYSTEM

The semiclassical treatment of the laser[1] relates the classical laser electromagnetic field with the quantum-mechanical polarization of the active medium.

Following the development of Refs. 1, 5, and 6 we consider the steady-state operation of a laser in a single longitudinal mode. The electric field at time t and axial position z is assumed to be given by (all fields are taken to be polarized in the x direction)

$$E(z,t) = E_0 \sin kz \cos \nu t, \tag{2.1}$$

where E_0 is the amplitude, ν is the angular frequency, and $k = m\pi/L$ (m is a very large integer) is the wave number. This field induces a polarization

$$P(z,t) = \mathcal{P}[C(z)\cos\nu t + S(z)\sin\nu t], \tag{2.2}$$

where $C(z)$ and $S(z)$ are in phase and quadrature coefficients and $\mathcal{P} = e\langle a|x|b\rangle$ is the electric dipole moment between excited states a and b. In the presence of the field the atoms experience an interaction perturbation

$$\hbar V(z,t) = -\mathcal{P}E(z,t), \tag{2.3}$$

which induces stimulated emission and absorption transitions between states a and b.

By taking the spatial Fourier projection of the wave equation on the cavity mode[1] (integrating with the factor $2L^{-1}\int_0^L dz \sin kz$) and equating coefficients of $\sin\nu t$ and $\cos\nu t$, one obtains the amplitude and frequency determining equations for steady-state operation

$$E_0 = -(Q/\epsilon_0)S \tag{2.4a}$$

and

$$(\nu - \Omega)E_0 = -(\nu/\epsilon_0)C, \tag{2.4b}$$

where

$$\begin{pmatrix} C \\ S \end{pmatrix} = \frac{2}{L}\int_0^L dz \sin kz \begin{pmatrix} C(z) \\ S(z) \end{pmatrix} \tag{2.5}$$

are the spatial Fourier projections of the in phase $C(z)$ and quadrature $S(z)$ polarization coefficients, ϵ_0 is the dielectric constant, and Q is the cavity mode "Q" value. The field frequency ν will be slightly shifted from the cavity frequency $\Omega = ck$ because of dispersion effects in the medium.

Before Eqs. (2.4) can be used to determine the amplitude and frequency, we first have to obtain C and S as functions of the field through a quantum-mechanical analysis of the interaction between the excited laser atoms and the field.

First we assume that the laser transition levels a and b (with energies $W_a > W_b$) are pumped at the rate

$$\lambda_\alpha(v) = \Lambda_\alpha W(v), \quad \alpha = a, b \tag{2.6}$$

where Λ_α is constant and $W(v)$ is assumed to be the normalized Maxwellian velocity distribution

$$W(v) = (u\sqrt{\pi})^{-1} e^{-v^2/u^2}, \tag{2.7}$$

where u is the most probable speed. This pumping rate density gives the density of atoms with axial velocity v that are excited to state α per unit time. These energy levels are assumed to decay to lower states with the constant rates γ_a and γ_b. Thus in the absence of the laser electromagnetic field the pumping results in a population inversion density

$$N_0(v) = \lambda_a(v)/\gamma_a - \lambda_b(v)/\gamma_b \tag{2.8}$$

and a total active atom density

$$M_0(v) = \lambda_a(v)/\gamma_a + \lambda_b(v)/\gamma_b \ . \tag{2.9}$$

In the presence of the laser field interaction-induced transitions change the relative populations of the active states a and b. This interaction is analyzed by using a classical ensemble averaged density matrix[6]:

$$\rho(v, z, t) = \begin{pmatrix} \rho_{aa}(v, z) & \rho_{ab}(v, z, t) \\ \rho_{ba}(v, z, t) & \rho_{bb}(v, z) \end{pmatrix}, \tag{2.10}$$

which describes an ensemble of atoms at z moving with axial velocity v. This density matrix satisfies the equation of motion

$$\left(\frac{\partial}{\partial t} + v\frac{\partial}{\partial z}\right)\rho(v, z, t) = \lambda(v) - i\hbar^{-1}[H(z, t), \rho(v, z, t)] - \tfrac{1}{2}\{\Gamma, \rho(v, z, t)\}, \tag{2.11}$$

where $[\ ]$ denotes the commutator and $\{\ \}$ denotes the anticommutator. The other quantities are the Hamiltonian

$$H(z, t) = \begin{pmatrix} W_a & \hbar V(z, t) \\ \hbar V(z, t) & W_b \end{pmatrix}, \tag{2.11a}$$

the pumping matrix

$$\lambda(v) = \begin{pmatrix} \lambda_a(v) & 0 \\ 0 & \lambda_b(v) \end{pmatrix}, \tag{2.11b}$$

and the decay matrix

$$\Gamma = \begin{pmatrix} \gamma_a & 0 \\ 0 & \gamma_b \end{pmatrix} \ . \tag{2.11c}$$

For steady-state operation the time dependence can be removed from the problem by taking out the optical frequency oscillations through the substitution[5]

$$\rho_{ab}(v, z, t) = \rho_1(v, z)e^{-i\nu t} \tag{2.12}$$

and neglecting terms with the rapid time variation $\exp(\pm 2i\nu t)$ (rotating-wave approximation). Writing out the elements of (2.11) [noting that $\rho_{ba}(v, z, t) = \rho^*_{ab}(v, z, t)$] we obtain

$$[v\partial/\partial z + i(\omega - \nu) + \gamma_{ab}]\rho_1(v, z) = i V(z, t)[\rho_{aa}(v, z) - \rho_{bb}(v, z)], \tag{2.13a}$$

$$(v\partial/\partial z + \gamma_a)\rho_{aa}(v, z) = \lambda_a(v) + i V(z)[\rho_1(v, z) - \rho_1^*(v, z)] \ , \tag{2.13b}$$

$$(v\partial/\partial z + \gamma_b)\rho_{bb}(v, z) = \lambda_b(v) - i V(z)[\rho_1(v, z) - \rho_1^*(v, z)], \tag{2.13c}$$

where $V(z) = (\mathcal{P}E_0/2\hbar)\sin kz$, $\gamma_{ab} = \frac{1}{2}(\gamma_a + \gamma_b)$, and $\omega = (W_a - W_b)/\hbar$.

The presence of collisions cause a broadening and shift of the atomic line shape which, in the simplest case, may be taken into account by the replacements[18] [in Eq. (2.13a)]

$$\gamma_{ab} \to \tilde{\gamma}_{ab} = \gamma_{ab} + \Delta\gamma_{ab} \tag{2.14a}$$

and

$$\omega \to \tilde{\omega} = \omega + \Delta\omega \ , \tag{2.14b}$$

where the velocity dependence of the modifications $\Delta\gamma_{ab}$ and $\Delta\omega$ has been neglected.

Solving Eq. (2.13) for the density matrix $\rho(v, z)$ enables us to determine the polarization and the transition-level populations as functions of the electric field. First we note that the contribution to the polarization due to each velocity ensemble is given by

$$P(v, z, t) = \mathcal{P}[\rho_{ab}(v, z, t) + \rho_{ba}(v, z, t)], \tag{2.15}$$

which, in analogy with Eq. (2.2), can be written as

$$P(v, z, t) = \mathcal{P}[C(v, z)\cos\nu t + S(v, z)\sin\nu t], \tag{2.16}$$

where [using Eq. (2.12)]

$$C(v, z) = 2\mathrm{Re}[\rho_1(v, z)] \tag{2.17a}$$

and

$$S(v, z) = 2\mathrm{Im}[\rho_1(v, z)] \ . \tag{2.17b}$$

These coefficients are related to the polarization coefficients $C(z)$ and $S(z)$ defined in (2.2) by

$$\begin{pmatrix} C(z) \\ S(z) \end{pmatrix} = \int_{-\infty}^{\infty} dv\, W(v) \begin{pmatrix} C(v,z) \\ S(v,z) \end{pmatrix} . \tag{2.18}$$

The spatially averaged cavity mode projections C and S, for use in the amplitude and frequency determining Eqs. (2.4), are then obtained by using Eq. (2.5).

The population inversion density and total active atom density in the presence of the field for a velocity ensemble with velocity v at the point z are given by

$$N(v,z) = \rho_{aa}(v,z) - \rho_{bb}(v,z) \tag{2.19a}$$

and

$$M(v,z) = \rho_{aa}(v,z) + \rho_{bb}(v,z) , \tag{2.19b}$$

respectively. In the absence of the field (e.g., below threshold) the population densities are given by (2.8) and (2.9).

Rather than solve Eq. (2.13) for the density matrix elements and then determine the desired quantities in (2.17) and (2.19), we transform Eq. (2.13) into a set of dimensionless differential equations which directly determine the desired populations and polarization coefficients. This is accomplished by introducing the dimensionless variable

$$y = kz \tag{2.20}$$

and the following dimensionless parameters:

$$K \equiv kv/\gamma_{ab} , \tag{2.21a}$$

the velocity parameter;

$$\delta \equiv (\tilde{\omega} - \nu)/\gamma_{ab} , \tag{2.21b}$$

the detuning parameter;

$$\gamma_c \equiv \tilde{\gamma}_{ab}/\gamma_{ab} = 1 + \Delta\gamma_{ab}/\gamma_{ab} , \tag{2.21c}$$

the collision parameter;

$$\gamma_d \equiv \frac{\gamma_a - \gamma_b}{\gamma_a + \gamma_b} = \frac{1 - \gamma_a/\gamma_b}{1 + \gamma_a/\gamma_b} \tag{2.21d}$$

or

$$\gamma_0^2 \equiv \gamma_a\gamma_b/\gamma_{ab}^2 = 1 - \gamma_d^2 , \tag{2.21e}$$

the level-decay-rate ratio parameters; and

$$I \equiv \mathcal{P}^2 E_0^2/(2\hbar^2\gamma_a\gamma_b) , \tag{2.21f}$$

the intensity or saturation parameter.

In terms of these dimensionless quantities Eq. (2.13) is transformed into the matrix differential equation

$$[Kd/dy + \Gamma(y)]\,\vec{\Delta}(y,K) = \vec{\Lambda} , \tag{2.22}$$

where the desired unknowns are

$$\vec{\Delta}(y,K) = \frac{1}{N_0}\begin{bmatrix} C(y,K) \\ S(y,K) \\ M(y,K) \\ N(y,K) \end{bmatrix} , \tag{2.23a}$$

the nonhomogeneous part

$$\vec{\Lambda} = \begin{bmatrix} 0 \\ 0 \\ M_0/N_0 + \gamma_d \\ 1 + \gamma_d M_0/N_0 \end{bmatrix} , \tag{2.23b}$$

and the coefficient matrix

$$\Gamma(y) = \begin{bmatrix} \gamma_c & -\delta & 0 & 0 \\ \delta & \gamma_c & 0 & (2I)^{1/2}\gamma_0 \sin y \\ 0 & 0 & 1 & \gamma_d \\ 0 & -(2I)^{1/2}\gamma_0 \sin y & \gamma_d & 1 \end{bmatrix} . \tag{2.23c}$$

Upon solving (2.22) for $\vec{\Delta}(y,K)$ the polarization and populations of an ensemble of atoms at axial position y with velocity K are obtained in terms of the field intensity, cavity detuning, decay rate ratio, and collision parameters. Similar information can also be obtained for the spatially averaged population densities and cavity mode projections of the polarization for each velocity ensemble by writing

$$\begin{aligned} \vec{\Delta}(K) &\equiv \frac{1}{N_0}\begin{bmatrix} C(K) \\ S(K) \\ M(K) \\ N(K) \end{bmatrix} \\ &= \frac{1}{2\pi N_0}\int_0^{2\pi} dy \begin{bmatrix} 2\sin y\, C(y,K) \\ 2\sin y\, S(y,K) \\ M(y,K) \\ N(y,K) \end{bmatrix} . \end{aligned} \tag{2.24}$$

With a knowledge of the polarization coefficients in (2.24) the coefficients C and S for use in the amplitude and frequency determining Eqs. (2.4) are obtained by integrating over all velocity ensembles, i.e.,

$$\vec{\Delta} = (\overline{K}\sqrt{\pi})^{-1}\int_{-\infty}^{\infty} dk\, e^{-(K/\overline{K})^2}\,\vec{\Delta}(K), \quad \overline{K} = ku/\gamma_{ab} \tag{2.25}$$

in analogy with Eq. (2.18).

III. METHODS OF SOLUTION

The solution of the laser equation (2.22) for steady-state single-mode operation can be accom-

plished by several methods. Some of the methods to be discussed will serve to relate previous laser theories and other new methods will provide improved analytic approximations and numerical solutions. It is to be expected that the new methods will also prove useful in related research areas including high-intensity multimode laser theory.

The boundary condition satisfied by physically acceptable solutions is obtained by some physical insight. Our assumed electric field (2.1) is basically periodic[19] with period 2π and

$$E(y+\pi) = -E(y)\,. \tag{3.1}$$

We thus expect that the polarization, which is induced by this field, will have the same periodic behavior. The population densities which depend on the field intensity will have the same periodic behavior as the intensity (i.e., the electric field squared) which is periodic with period π.

The periodic boundary condition satisfied by $\vec{\Delta}(y,K)$ can thus be written as

$$\vec{\Delta}(y+2\pi,K) = \vec{\Delta}(y,K) \tag{3.2a}$$

and

$$\vec{\Delta}(y+\pi,K) = \begin{bmatrix} -1 & & 0 \\ & -1 & \\ & & 1 \\ 0 & & & 1 \end{bmatrix} \vec{\Delta}(y,K) \equiv E_2 \vec{\Delta}(y,K). \tag{3.2b}$$

First we see that for a stationary atom laser, e.g., a solid-state laser, Eq. (2.22) reduces (by setting $K=0$) to the algebraic equation

$$\Gamma(y)\vec{\Delta}(y,0) = \vec{\Lambda} \tag{3.3}$$

with the solution

$$\vec{\Delta}(y,0) = \Gamma^{-1}(y)\vec{\Lambda} = \frac{1}{1+2I\gamma_c \mathfrak{L}\sin^2 y} \begin{bmatrix} -\delta\gamma_0(2I)^{1/2}\mathfrak{L}\sin y \\ -\gamma_c\gamma_0(2I)^{1/2}\mathfrak{L}\sin y \\ (1+2I\gamma_c\mathfrak{L}\sin^2 y)(M_0/N_0+\gamma_d)-\gamma_d \\ 1 \end{bmatrix}, \tag{3.4}$$

where

$$\mathfrak{L} = (\gamma_c^2+\delta^2)^{-1} \tag{3.5}$$

is a dimensionless Lorentzian and the collision parameter γ_c [Eq. (2.21c)] now represents spin-lattice relaxation broadening.[20] The solution (3.4) clearly satisfies the periodic boundary condition (3.2). The spatially averaged quantities $\vec{\Delta}(K=0)$ defined in Eq. (2.24) are obtained by direct integration [Ref. 21, Eq. (3.681) and Ref. 22, Eq. (15.1.14)] to give

$$\vec{\Delta}(K=0) = \begin{bmatrix} -2\delta\gamma_0\gamma_c^{-1}(2I)^{-1/2}[1-(1+2I\gamma_c\mathfrak{L})^{-1/2}] \\ -2\gamma_0(2I)^{-1/2}[1-(1+2I\gamma_c\mathfrak{L})^{-1/2}] \\ M_0/N_0+\gamma_d[1-(1+2I\gamma_c\mathfrak{L})^{-1/2}] \\ (1+2I\gamma_c\mathfrak{L})^{-1/2} \end{bmatrix}. \tag{3.6}$$

When the motion of the atoms cannot be neglected the complete differential equation (2.22) has to be solved. There are several methods which can accomplish this solution.

First, we note that

$$K\frac{d}{dy}\left[\exp\left(\int \Gamma\, dy/K\right)\right] \equiv K\frac{d}{dy}\left[\sum_{n=0}^{\infty}\frac{1}{n!}\left(\int \Gamma\, dy/K\right)^n\right]$$
$$= \Gamma\exp\left(\int \Gamma\, dy/K\right)$$
$$= \exp\left(\int \Gamma\, dy/K\right)\Gamma \tag{3.7}$$

if and only if $\Gamma(y)$ commutes with its integral, i.e.,

$$\left[\Gamma(y), \int \Gamma(y)\,dy\right] = 0. \tag{3.8}$$

Thus the general solution of Eq. (2.22) can be written as[23-25]

$$\vec{\Delta}(y,K) = \exp\left(-\int \Gamma\, dy/K\right) \times\left[\vec{c}+\int_{y_0}^{y} dy' \exp\left(\int \Gamma\, dy'/K\right)\vec{\Lambda}/K\right] \tag{3.9}$$

if and only if[23] Eq. (3.8) is satisfied. Here $\vec{c}$ is a constant vector of integration and y_0 is an arbitrary lower integration limit. The quantity

$$\vec{\Delta}(y_0,K) = \exp\left(-\int^{y_0}\Gamma\, dy/K\right)\vec{c} \tag{3.10}$$

is the initial value of $\vec{\Delta}(y,K)$ at $y=y_0$. However, since we do not *a priori* know the value of $\vec{\Delta}(y,K)$ at any point, we will choose y_0 to be an arbitrary convenient point and determine $\vec{c}$ from the periodic boundary condition Eq. (3.2).

For $\Gamma(y)$ defined in (2.23c), condition (3.8) will be satisfied and (3.9) will be the desired solution when (aside from the trivial case $I=0$)

$$\delta=0, \quad \gamma_d=0, \quad \text{and } \gamma_c=1, \tag{3.11}$$

i.e., for zero detuning, equal level decay rates, and neglecting collision broadening.

The evaluation of (3.9) for the special case (3.11) in Secs. IV and V results in a definite integral solution which can be integrated analytically in terms of Bessel functions. The results also serve to relate previous exact solutions for this special case.[6,14-16]

For general single-mode operation, when $\Gamma(y)$ does not commute with its integral we can get a formal solution similar to (3.9) by separating $\Gamma(y)$ into two parts,

$$\Gamma(y)=\Gamma_1+\Gamma_2, \tag{3.12}$$

where Γ_1 commutes with its integral. Since every constant matrix commutes with its integral a convenient choice would be to let Γ_1 contain the constant elements of $\Gamma(y)$, and Γ_2 the y-dependent elements. Equation (2.32) can then be written as

$$(Kd/dy+\Gamma_1)\vec{\Delta}(y,K)=\vec{\Lambda}-\Gamma_2\vec{\Delta}(y,K) \tag{3.13}$$

with the solution

$$\vec{\Delta}(y,K)=\exp\left(-\int\Gamma_1\,dy/K\right)\left[\vec{c}+\int_{y_0}^{y}dy'\exp\left(\int\Gamma_1\,dy'/K\right)\times[\vec{\Lambda}-\Gamma_2\vec{\Delta}(y',K)]\Big/K\right]. \tag{3.14}$$

This formal matrix integral equation solution can be evaluated by successive iterations to obtain the Neumann series solution.[26] This series is slowly converging for high intensities but improved approximations can be obtained by taking the Padé approximants[27,28] to the Neumann series. However, as we will discuss below, we have much better methods for obtaining numerical results and analytic approximations for general single-mode operation. Thus the primary usefulness of (3.14) is in the insight that may be obtained from the integral equations which are similar to the integral equations that represent Mathieu functions.[19]

A related approach is to diagonalize the coefficient matrix through a similarity transformation of Eq. (2.22), i.e.,

$$K\frac{d\vec{\Delta}'}{dy}+\left(KU^{-1}\frac{dU}{dy}+U^{-1}\Gamma U\right)\vec{\Delta}'=U^{-1}\vec{\Lambda}, \tag{3.15}$$

where $\vec{\Delta}=U\vec{\Delta}'$ and $U^{-1}\Gamma U$ is diagonal; a solution in the form of Eq. (3.9) can then be obtained if the term $KU^{-1}dU/dy$ is diagonal or can be neglected. It turns out that Γ can be diagonalized by a constant matrix U, and hence $KU^{-1}dU/dy=0$, only for the special case of Eq. (3.11). For the general case it does not lead to an exact solution but can lead to different approximations by neglecting the $KU^{-1}dU/dy$ term. Another approximation can be obtained by neglecting the noncommutivity of Γ and writing Eq. (3.9) as the solution. These additional methods do not lead to especially useful results in the present research.

We can also solve the differential equation (2.22) directly by numerical methods. The most advantageous methods for the direct numerical solution of differential equations[29] are the forward integration methods such as Runga-Kutta and predictor-corrector techniques. However, these methods are designed for solving initial-value problems (i.e., they require the knowledge of the solution at an initial value in the order to be able to start the forward integration routine). Since we do not *a priori* know the value of $\vec{\Delta}(y,K)$ at any y, we first have to use the periodic boundary condition (3.2) to obtain an initial value $\vec{\Delta}(y_0,K)$ at a convenient $y=y_0$. This is accomplished by the method of Goodman and Lance,[30] which enables one to numerically convert two point boundary-value problems to initial-value problems. This method will be discussed in more detail in Sec. VII.

The best means for obtaining exact numerical results and analytic approximations is to expand the solution in a Fourier series and solve the resulting recursion relations for the coefficients. These recursion relations have previously been solved[5-7] by using a continued fraction whose convergence properties have been proven analytically.[8] The problem of round-off errors in the direct evaluation of the continued fraction is eliminated by using the method of successive convergents.[9,29] However, backward recurrence techniques generally have better convergence properties in numerical evaluation than continued fractions[31] as has also recently been found in the development of a multimode unidirectional traveling-wave laser theory.[32] Thus in Sec. VIII we develop a backward recurrence scheme for solving the recursion relations for the Fourier series coefficients, and also find that the best analytic approximations are obtained by analytically evaluating the coefficients in truncated Fourier series solutions.

IV. EXACT INTEGRAL SOLUTION FOR SPECIAL CASE

As discussed in Sec. III, an exact integral solution can be obtained when condition (3.8) is satis-

fied; i.e., when the detuning is zero, the level decay rates are equal, and we neglect collision broadening [Eq. (3.11)]. In this section we obtain this solution as presented by previous authors,[14-16] and, through the reduction of the integration limits and other manipulations, integrate the solution analytically in terms of Bessel functions. The results thus obtained are equivalent to the Bessel function solution obtained by Feldman and Feld[6] for this special case through the analytic evaluation of the recursion relations for the Fourier coefficients.

In addition we will obtain a solution in the form of a series of Bessel functions of integer order which provides a method for predicting the positions of the secondary resonance in graphs of $N(K)$ vs K. The first term in this series is the result obtained by Rautian and Sobelman[14] for this case.

We will thus relate the different approaches to the solution and add some additional insight to the problem.

When $\delta = 0$, $\gamma_d = 0$, and $\gamma_c = 1$ the differential equations for $C(y,K)$ and $M(y,K)$ in Eq. (2.22) become decoupled and directly integrable. The solution, subject to the boundary condition (3.2), is

$$C(y,K) = 0 \tag{4.1a}$$

and

$$M(y,K) = M_0. \tag{4.1b}$$

The coupled equations for $S(y,K)$ and $N(y,K)$ become

$$[Kd/dy + \Gamma_s(y)]\vec{\Delta}_s(y,K) = \vec{\Lambda}_s, \tag{4.2}$$

where

$$\vec{\Delta}_s(y,K) \equiv \frac{1}{N_0}\begin{pmatrix} S(y,K) \\ N(y,K) \end{pmatrix}, \tag{4.3a}$$

$$\vec{\Lambda}_s \equiv \begin{pmatrix} 0 \\ 1 \end{pmatrix}, \tag{4.3b}$$

and

$$\Gamma_s(y) = \begin{pmatrix} 1 & (2I)^{1/2}\sin y \\ -(2I)^{1/2}\sin y & 1 \end{pmatrix}. \tag{4.3c}$$

Since Γ_s commutes with its integral the solution of (4.2) is

$$\vec{\Delta}_s(y,K) = \exp\left(-\int \Gamma_s dy/K\right) \times\left[\vec{c} + \int_{y_0}^{y} dy' \exp\left(\int \Gamma_s dy'/K\right)\vec{\Lambda}_s/K\right]. \tag{4.4}$$

A useful method for determining the exponential of the matrix $\int \Gamma_s dy/K$ is to use the Cayley-Hamilton theorem[24, 33] which enables one to write any function of an $n \times n$-order matrix as an $(n-1)$-degree polynomial in the matrix. For the 2×2 matrix Γ_s this gives

$$\exp\left(\int \Gamma_s dy/K\right) = \alpha_0 E + \alpha_1\left(\int \Gamma_s dy/K\right), \tag{4.5}$$

where E is the identity matrix. The eigenvalues of the matrix satisfy the same functional relationship as the matrix or

$$e^u = \alpha_0 + \alpha_1 u, \tag{4.6}$$

where the eigenvalues $u = [y \pm i(2I)^{1/2}\cos y]/K$. Evaluating (4.6) for the coefficients α_0 and α_1 and substituting in (4.5) we obtain

$$\exp\left(\int \Gamma_s dy/K\right) = e^{y/K}\begin{pmatrix} \cos(\chi\cos y) & -\sin(\chi\cos y) \\ \sin(\chi\cos y) & \cos(\chi\cos y) \end{pmatrix}, \tag{4.7a}$$

where

$$\chi = (2I)^{1/2}K^{-1}, \tag{4.7b}$$

and where $\exp(-\int \Gamma_s dy/K)$ is obtained by substituting $-K$ for K in (4.7).

The determination of the constant of integration $\vec{c}$ in (4.4) for an arbitrary choice of lower integration limit y_0 requires the use of the periodic boundary condition (3.2).

By choosing $y_0 = -\infty$ and substituting (4.4) in (3.2a) (making the change of variable $y'' = y' - 2\pi$ in the right-hand side we obtain $\vec{c} = 0$. The solution (4.4) then becomes

$$\Delta_s(y,K) = \frac{1}{K}\int_0^\infty d\hat{y}\, e^{-\hat{y}/K}\begin{pmatrix} \sin\{\chi(\cos y - \cos[y-\hat{y}])\} \\ \cos\{\chi(\cos y - \cos[y-\hat{y}])\} \end{pmatrix}, \tag{4.8}$$

where $\hat{y} = y - y'$. This is equivalent to the results obtained by Refs. 14–16.

However by noting that (4.8) is the Laplace transform of a periodic function (of period 2π in $\hat{y}$) it can be put into a much more suitable form for evaluation. The property of such a transform [Ref. 22, Eq. (29.2.16)] is

$$f(s) = \int_0^\infty e^{-st}F(t)\,dt = (1 - e^{-2\pi s})^{-1}\int_0^{2\pi} e^{-st}F(t)\,dt \tag{4.9a}$$

when

$$F(t + 2\pi) = F(t). \tag{4.9b}$$

Hence the solution (4.8b) reduces immediately to

$$\vec{\Delta}_s(y,K)=\frac{1}{K(1-e^{-2\pi s})}\times\int_0^{2\pi}d\hat{y}\,e^{-\hat{y}/K}\begin{pmatrix}\sin\{\chi(\cos y-\cos[y-\hat{y}])\}\\ \cos\{\chi(\cos y-\cos[y-\hat{y}])\}\end{pmatrix}. \tag{4.10}$$

The reduced integration region simplifies the numerical integration of this solution and enables one to integrate this solution analytically in terms of Bessel functions (see Sec. V).

Another solution is obtained by choosing $y_0=0$ as the arbitrary lower integration limit in (4.4). Imposing the periodic boundary condition (3.2a) on the solution we obtain

$$\vec{c}=\frac{1}{K(e^{-2\pi/K}-1)}\int_0^{2\pi}dy'\,e^{y'/K}\begin{pmatrix}-\sin(\chi\cos y')\\ \cos(\chi\cos y')\end{pmatrix}. \tag{4.11}$$

Hence the solution (4.4) becomes

$$\vec{\Delta}_s(y,K)=\frac{1}{K}\exp\left(-\int\Gamma_s\,dy/K\right)\times\left((e^{2\pi/K}-1)^{-1}\int_0^{2\pi}dy'+\int_0^{y}dy'\right)\times e^{y'/K}\begin{pmatrix}-\sin(\chi\cos y')\\ \cos(\chi\cos y')\end{pmatrix}, \tag{4.12}$$

where $\exp(-\int\Gamma_s dy/K)$ is obtained from Eq. (4.7). As discussed below this form of the solution is more suitable than (4.10) for numerical integration. Equation (4.12) will also be used in Sec. V to obtain a Bessel function series solution which provides a method for predicting the position of depletion resonances in the spatially averaged population inversion density.

The solution (4.12) is more suitable than (4.10) for numerical integration using trapezoidal or Simpson's method because the integrand does not depend on y. This means that (4.12) only has to be integrated once—from 0 to y, increasing y incrementally from 0 to 2π, and adding the incremental integral to the previous value—to get the value of the integral at each incrementally spaced y in the period. When y reaches 2π we automatically obtain $\int_0^{2\pi}dy'$ and the integration is completed. In contrast the integration of (4.10) requires a separate integration from 0 to 2π for each value of y because when y is changed the integrand is changed.

After the integrals in (4.12) are evaluated to obtain $\vec{\Delta}_s(y,K)$ at incrementally spaced y, the spatially averaged quantities $S(K)$ and $N(K)$ defined in (2.4) are obtained by integrating $\vec{\Delta}_s(y,K)$ using trapezoidal or Simpson's method.

A listing of the computer program which integrates (4.12) is given in Appendix B of Ref. 17. The time required to calculate $N(y,K)$ and $S(y,K)$ for 100 increments in y and then $N(K)$ and $S(K)$ was about 0.2 sec. By contrast the integration of (4.1), where the integrand depends on y, required about 2.5 sec for each K.

Before ending this section it should be pointed out that (4.12) can be reduced to (4.10) directly by algebraic manipulations. Multiplying the integrand in (4.12) by the coefficient matrix $\exp(\int\Gamma_s dy/K)$, combining the two integrals by writing

$$(e^{2\pi/K}-1)^{-1}\int_0^{2\pi}dy'+\int_0^{y}dy'=(1-e^{-2\pi/K})^{-1}\left(\int_0^{y}dy'+e^{-2\pi/K}\int_y^{2\pi}dy'\right), \tag{4.13}$$

and substituting $y'=y-\hat{y}$ in the first integral and $y'=y-\hat{y}+2\pi$ in the second integral, the solution (4.12) reduces to (4.10).

V. ANALYTIC EVALUATION OF EXACT SOLUTION

We will now analytically integrate the exact integral solutions of Sec. IV for the special case $\delta=0$, $\gamma_a=\gamma_b$, and $\gamma_c=1$ to give exact analytic solutions in terms of Bessel functions.

By writing the cosine terms in the integrand of (4.10) as

$$\cos y-\cos(y-\hat{y})=2\sin y'\sin(y-y'), \tag{5.1}$$

where $y'=2\hat{y}$, the integrand can be expanded in terms of Bessel functions of complex order [Ref. 22, (9.1.42) and (9.1.43)], to give

$$\vec{\Delta}_s(y,K)=2K^{-1}(1-e^{-2\pi/K})^{-1}\sum_{m=0}^{\infty}\int_0^{\pi}dy'e^{-2y'/K}\begin{pmatrix}-\epsilon_{2m+1}J_{2m+1}(2\chi\sin y')\sin[(2m+1)(y-y')]\\ \epsilon_{2m}J_{2m}(2\chi\sin y')\cos[2m(y-y')]\end{pmatrix} \tag{5.2a}$$

$$=\frac{\pi}{K}\operatorname{csch}\left(\frac{\pi}{K}\right)\sum_{m=0}^{\infty}\begin{pmatrix}\mathrm{Re}[e^{i(2m+1)y}J_{2m+1-i/K}(\chi)J_{i/K}(\chi)]\\ \mathrm{Im}[e^{i2my}J_{2m-i/K}(\chi)J_{i/K}(\chi)]\end{pmatrix} \tag{5.2b}$$

where $\epsilon_n \equiv (1,\ \text{for } n=0;\ 2,\ \text{for } n\geq 1)$ is Neumann's factor,[34] $\chi = (2I)^{1/2}K^{-1}$, and where we used $J_{\nu *}(\chi) = [J_\nu(\chi)]^*$.

The spatially averaged quantities $S(K)$ and $N(K)$ are obtained by integrating (5.2b) [Ref. 21, Eqs. (3.891)] to give

$$\vec{\Delta}_s(K) = \frac{1}{N_0}\begin{pmatrix} S(K) \\ N(K) \end{pmatrix} = \frac{\pi}{K}\operatorname{csch}\left(\frac{\pi}{K}\right)\begin{pmatrix} -2\operatorname{Im}[J_{1-i/K}(\chi)J_{i/K}(\chi)] \\ |J_{i/K}(\chi)|^2 \end{pmatrix}. \quad (5.3)$$

This result is equivalent to the result obtained by Feldman and Feld[6] [Eq. (88)] who were able to sum the recursion relations analytically for this special case. The equivalence is obtained by using the Wronskian and recursion relations for Bessel functions [Ref. 22, Eqs. (9.1.15) and (9.1.27)] to obtain

$$(\pi/K)\operatorname{csch}(\pi/K) = |J_{i/K}(\chi)|^{-2}\left[1 + (2I)^{1/2}\operatorname{Im}\left(\frac{J_{1-i/K}(\chi)}{J_{-i/K}(\chi)}\right)\right]^{-1}. \quad (5.4)$$

By expanding the product of Bessel functions in (5.3) [Ref. 22, Eq. (9.1.14)] we can also obtain the series solution

$$\vec{\Delta}_s(K) = \frac{\pi}{K}\operatorname{csch}\left(\frac{\pi}{K}\right) \times \sum_{m=0}^{\infty} \frac{(-1)^m(\chi/2)^{2m}(2m)!}{(m!)^2\Gamma(m+1+i/K)\Gamma(m+1-i/K)} \times \begin{pmatrix} \dfrac{-(2m+1)(2I)^{1/2}}{(m+1)[1+(m+1)^2K^2]} \\ 1 \end{pmatrix} \quad (5.5a)$$

$$= \sum_{m=0}^{\infty} \frac{(-I/2)^m(2m)!}{(m!)^2(1+K^2)(1+2^2K^2\cdots(1+m^2K^2)} \times \begin{pmatrix} \dfrac{-(2m+1)(2I)^{1/2}}{(m+1)[1+(m+1)^2K^2]} \\ 1 \end{pmatrix}, \quad (5.5b)$$

where the gamma functions in (5.5a) were expanded using Ref. 22, Eqs. (6.1.15) and (6.1.31). This last expansion for $N(K)$ is the one obtained by Stenholm[15] [Eq. 43]. For $K>0$ it converges for all I—rapidly for large K, slowly for small K. When $K=0$ it reduces to the expansion of the exact solution (3.6) for $I<0.5$ and diverges for larger I.

Another Bessel function solution is obtained from solution (4.12). As before, if the integrand in (4.12) is expanded in terms of Bessel functions [Ref. 22, Eqs. (9.1.44-45)] it can be integrated to give

$$\vec{\Delta}_s(y,K) = \exp\left(-\int \Gamma_s dy/K\right)\sum_{n=0}^{\infty}(-1)^n \begin{pmatrix} -\epsilon_{2n+1}J_{2n+1}(\chi)\mathfrak{M}_{2n+1}\{\cos[(2n+1)y] + (2n+1)K\sin[(2n+1)y]\} \\ \epsilon_{2n}J_{2n}(\chi)\mathfrak{M}_{2n}\{\cos 2ny + 2nK\sin 2ny\} \end{pmatrix}, \quad (5.6)$$

where the Lorentzian $\mathfrak{M}_n = (1+n^2K^2)^{-1}$, and $\exp(-\int \Gamma_s dy/K)$ is given by (4.7).

The spatially averaged quantities are obtained by direct integration using (Ref. 19, Appendix B)

$$\frac{1}{2\pi}\int_0^{2\pi}\sin(z\cos y)\cos ny\,dy = \begin{cases}(-1)^{(n-1)/2}J_n(z), & n \text{ odd} \\ 0, & n \text{ even}\end{cases} \quad (5.7a)$$

$$\frac{1}{2\pi}\int_0^{2\pi}\cos(z\cos y)\cos ny\,dy = \begin{cases}(-1)^{n/2}J_n(z), & n \text{ even} \\ 0, & n \text{ odd}\end{cases}$$

and

$$\frac{1}{2\pi}\int_0^{2\pi}\sin(z\cos y)\sin ny\,dy = 0,$$

$$\frac{1}{2\pi}\int_0^{2\pi}\cos(z\cos y)\sin ny\,dy = 0. \quad (5.7b)$$

The result is

$$\frac{1}{N_0}\begin{pmatrix} S(K) \\ N(K) \end{pmatrix} = \begin{pmatrix} 0 \\ J_0^2(\chi) \end{pmatrix} + 2\sum_{n=1}^{\infty}\frac{J_n^2(\chi)}{1+n^2K^2}\begin{pmatrix} -2n^2K/\chi \\ 1 \end{pmatrix}. \quad (5.8)$$

The first term in this series, $J_0^2(\chi)$, is the solution obtained by Rautian and Sobelman.[14] It is clear from Fig. 1, [and implicit in Eq. (5.8)], that, as the intensity I becomes very large, the exact solution approaches $J_0^2(\chi)$. For smaller intensities the additional terms have to be added to get the correct magnitude of $N(K)$. However, an interesting result is the fact that the depletion resonances in $N(K)$ occur near the zeros of $J_0(\chi)$ for $I\gtrsim 1$ because the higher-order terms do not shift the position of the resonances appreciably in that case. A good approximation for the zeros of $J_0(\chi)$ (accurate to two significant digits[35]) which serves as a prediction for the resonance position is

$$K = (2I)^{1/2}[\tfrac{1}{4}\pi(4m-1)]^{-1}, \quad (5.9)$$

where m is an integer.

VI. INTEGRAL EQUATION SOLUTION FOR GENERAL CASE

As was shown in Sec. III we cannot obtain an exact analytic solution for the general single-mode gas laser. However, a solution in the form of an integral equation can be obtained by separating the coefficient matrix into two parts, one of which

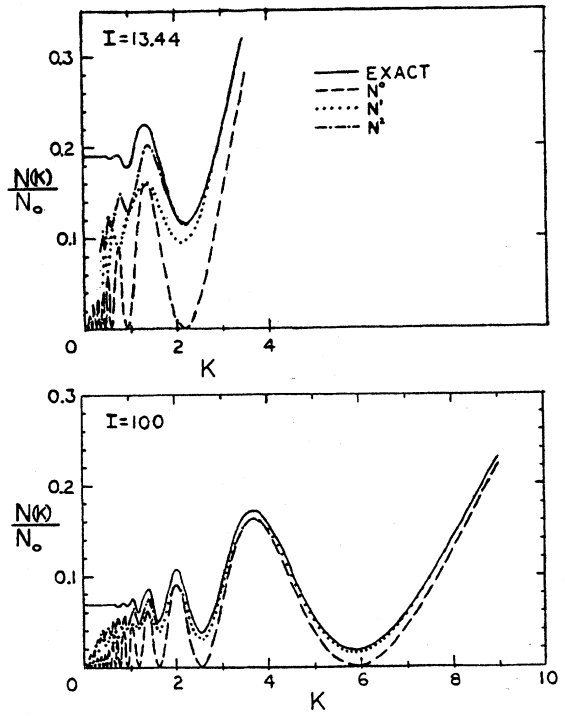

FIG. 1. Graphs of the population inversion density $N(K)$ as a function of atomic velocity K for the special case of zero detuning, equal level decay rates, and neglecting collision broadening comparing the exact solution and the approximation obtained by taking the first, N^0, first and second, N^1, and first three terms, N^2, in the Bessel series solution, Eq. (5.8). It becomes apparent that the depletion resonances in $N(K)$ occur at the zeros of the first term $J_0^2[(21)^{1/2}/K]$.

commutes with its integral. The resulting integral equation correctly includes the parameters in the commuting matrix and provides an iterated series for the parameters in the noncommuting part.

For obtaining exact numerical results and analytic approximations for the single-mode laser, the iteration of the integral equation is much slower and more cumbersome than the methods to be presented in Secs. VII and VIII. However, the integral equation solution is similar to the integral equation representations of Mathieu functions which provide insight into the properties of Mathieu functions. In addition, in a "dressed atom" approach[36] we are able to obtain predictions for the depletion resonance positions through a similar division of the coefficient matrix and analysis of the eigenvalues of the commuting matrix. We will therefore briefly present the integral equation solution for the general single-mode gas laser.

If we separate Γ into constant and y-dependent parts, i.e., $\Gamma(y)=\Gamma_1+\Gamma_2(y)$ then the integral equation solution (3.14) becomes

$$\vec{\Delta}(y,K)=e^{-\Gamma_1 y/K}\times\left(\vec{c}+\int_{y_0}^{y}dy'\,e^{\Gamma_1 y'/K}[\vec{\Lambda}-\Gamma_2(y')\vec{\Delta}(y',K)]/K\right), \tag{6.1}$$

where y_0 is arbitrary, $\vec{c}$ is evaluated from the boundary condition (3.2), and where

$$e^{\Gamma_1 y/K}=\begin{pmatrix} e^{\Gamma_{1a}y/K} & 0 \\ 0 & e^{\Gamma_{1b}y/K}\end{pmatrix} \tag{6.2}$$

with

$$e^{\Gamma_{1a}y/K}=e^{\gamma_c y/K}\begin{pmatrix}\cos(\delta y/K) & -\sin(\delta y/K)\\ \sin(\delta y/K) & \cos(\delta y/K)\end{pmatrix} \tag{6.3a}$$

and

$$e^{\Gamma_{1b}y/K}=e^{y/K}\begin{pmatrix}\cosh(\gamma_d y/K) & \sinh(\gamma_d y/K)\\ \sinh(\gamma_d y/K) & \cosh(\gamma_d y/K)\end{pmatrix}. \tag{6.3b}$$

The integral equation solution can thus be given by

$$\vec{\Delta}(y,K)=\begin{pmatrix}0\\0\\M_0/N_0\\0\end{pmatrix}-\frac{\chi\gamma_0}{N_0}\int_{-\infty}^{y}dy'\,\mathrm{sin}y'\begin{bmatrix}e^{-\gamma_c(y-y')/K}\sin[\delta(y-y')/K]N(y',K)\\ e^{-\gamma_c(y-y')/K}\cos[\delta(y-y')/K]N(y',K)\\ e^{-(y-y')/K}\sinh[\gamma_d(y-y')/K]S(y',K)\\ -e^{-(y-y')/K}\cosh[\gamma_d(y-y')/K]S(y',K)\end{bmatrix} \tag{6.4a}$$

or

$$\vec{\Delta}(y,K)=\begin{pmatrix}0\\0\\M_0/N_0\\0\end{pmatrix}+\frac{\chi\gamma_0}{N_0}e^{-\Gamma_1 y/K}\left((e^{\Gamma_1\pi/K}E_2-E)^{-1}\int_0^{\pi}dy'+\int_0^{y}dy'\right)\mathrm{sin}y'\begin{bmatrix}e^{\gamma_c y'/K}\sin(\delta y'/K)N(y',K)\\ -e^{\gamma_c y'/K}\cos(\delta y'/K)N(y',K)\\ e^{y'/K}\sinh(\gamma_d y'/K)S(y',K)\\ e^{y'/K}\cosh(\gamma_d y'/K)S(y',K)\end{bmatrix}, \tag{6.4b}$$

where E is the identity matrix and E_2 is defined in (3.2b).

We note that Eqs. (6.4) contain a set of coupled integral equations for $N(y,K)$ and $S(y,K)$ which are decoupled from the equations for $C(y,K)$ and $M(y,K)$. Thus even in the general case of single-mode operation we only have to solve the integral equations for $N(y,K)$ and $S(y,K)$ with $C(y,K)$ and $M(y,K)$ being obtained by integrating over the solutions for $N(y,K)$ and $S(y,K)$, respectively.

Another point which becomes apparent from (6.4) is that C, S, and N only depend on N_0, the pumped population inversion density, and are independent of the pumped total active atom density M_0.

VII. DIRECT NUMERICAL SOLUTION

An exact numerical solution for general single-mode operation can be obtained by solving Eq. (2.22) directly using numerical methods (Sec. III). Before forward integration techniques such as Runga-Kutta and predictor-corrector methods can be used to solve the differential equation, we have to convert the periodic boundary problem [Eq. (3.2)] to an initial-value problem. This is accomplished by using the method of Goodman and Lance[30] as discussed below.

We set up a matrix differential equation adjoint to Eq. (2.22) by writing

$$[Kd/dy - \Gamma^{\dagger}(y)]\Phi(y) = 0\,, \tag{7.1}$$

where $\Gamma^{\dagger}(y)$ is the adjoint, or conjugate transpose, of $\Gamma(y)$ and where $\Phi(y)$ is a matrix of order 4×4 that satisfies the initial condition

$$\Phi(0) = E\,, \tag{7.2}$$

where E is the identity matrix. Using (7.1) and (2.22) it is seen that

$$K(d/dy)[\Phi^{\dagger}(y)\vec{\Delta}(y,K)] = \Phi^{\dagger}(-\Gamma\vec{\Delta}+\vec{\Lambda}) + (\Gamma^{\dagger}\Phi)^{\dagger} = \Phi^{\dagger}\vec{\Delta}\,. \tag{7.3}$$

Integrating (7.3) from 0 to π we obtain

$$\Phi^{\dagger}(\pi)\vec{\Delta}(\pi,K) - \Phi^{\dagger}(0)\vec{\Delta}(0,K) = K^{-1}\int_0^{\pi} dy\,\Phi^{\dagger}(y)\vec{\Lambda}\,, \tag{7.4}$$

which reduces to

$$[\Phi^{\dagger}(\pi)E_2 - E]\vec{\Delta}(0,K) = K^{-1}\int_0^{\pi} dy\,\Phi(y)\vec{\Lambda} \tag{7.5}$$

with the use of the initial condition (7.1) for $\Phi(0)$ and the periodic boundary condition (3.2b) for $\vec{\Delta}(y,K)$.

Thus in order to obtain a numerical solution for Eq. (2.22) we solve the adjoint matrix differential equation (7.1) as an initial-value problem (7.2) using Runga-Kutta and predictor-corrector techniques. With a knowledge of $\Phi(y)$ at incrementally spaced values of $0 \leq y \leq \pi$ we can evaluate the integral in (7.5) using standard trapezoidal or Simpson methods and solve the resulting algebraic matrix equation for the initial value $\vec{\Delta}(0,K)$. Finally Eq. (2.22) can then be solved numerically as an initial-value problem.

A listing of the computer program which accomplishes the above integration is given in Appendix D of Ref. 17. The subroutines which numerically convert two-point boundary problems to initial-value problems and solve the differential equation are from the IBM Scientific Subroutine Package Library at the ERDA Computing Center at New York University.

The computing time required to solve for $\vec{\Delta}(y,K)$ in the region $0 \leq y \leq \pi$ and then find $\vec{\Delta}(K)$ by numerical integration was about 0.2 sec for each value of K. As we will see in Sec. VIII the evaluation of the Fourier series solution is about 40 times faster in calculating $\vec{\Delta}(K)$. However, the direct numerical solution may prove useful and applicable in obtaining solutions for other problems such as the high-intensity multimode laser.

VIII. FOURIER SERIES METHOD

As discussed in Sec. III the Fourier series method has been used[5-7] to obtain approximations and exact numerical solutions for the general single-mode laser. In this method we substitute a Fourier series for the desired quantities and obtain a recursion relation between the coefficients. These recursion relations have been solved by previous authors[5-7] using continued fraction methods. Kuroda and Ogura[8] have proven the convergence of the continued fraction but did not consider the roundoff errors introduced by the repeated divisions in the direct evaluation of the continued fraction. In this section we will develop a backward recurrence scheme for solving the recursion relations similar to the method[37] which has proved so successful in the evaluation of Bessel functions. This method uses additions and subtractions to evaluate the recursion relation, which is faster and less prone to roundoff errors than the direct evaluation of the continued fraction. However, evaluating the continued fraction by using recurrence relations for successive convergents[9,29] eliminates the time consumption and roundoff problem. It turns out that the method of successive convergents and the backward recurrence scheme are the best (fastest and most accurate) means for obtaining numerical results for the general single-mode standing-wave laser.

The desired quantities $S(y,K)$ and $N(y,K)$ are expanded in a spatial Fourier series by writing[5,6]

$$S(y,K)=N_0\sum_{n'=-\infty}^{\infty}{}' s_{n'}e^{in'y}, \quad n' \text{ an odd integer} \tag{8.1a}$$

and

$$N(y,K)=N_0\sum_{n''=-\infty}^{\infty}{}'' d_{n''}e^{in''y}, \quad n'' \text{ an even integer} \tag{8.1b}$$

where, since $S(y,K)$ and $N(y,K)$ are real,

$$s_{-n'}=s_{n'}^*, \quad d_{-n''}=d_{n''}^*, \quad d_0 \text{ real}. \tag{8.2}$$

Substituting (8.1) into the coupled integral equations[38] (6.4a) for $S(y,K)$ and $N(y,K)$, integrating, and equating coefficients of e^{iny} we obtain the recursion relations

$$s_{n'}=-i(I/8)^{1/2}\gamma_0(L_{n'}^{+}+L_{n'}^{-})(d_{n'+1}-d_{n'-1}) \tag{8.3a}$$

and

$$d_{n''}=i(I/8)^{1/2}\gamma_0(M_{n''}^{+}+M_{n''}^{-})(s_{n''+1}-s_{n''-1})+\delta_{n'',0}, \tag{8.3b}$$

where

$$L_{n'}^{\pm}=[\gamma_0+i(n'K\pm\delta)]^{-1}, \quad L_{-n'}^{\pm}=L_{n'}^{\mp *}, \tag{8.4a}$$

$$\begin{aligned} M_{n''}^{+}&=[1+\gamma_d+in''K]^{-1}=\gamma_{ab}[\gamma_a+in''Kv]^{-1} \\ M_{n''}^{-}&=[1-\gamma_d+in''K]^{-1}=\gamma_{ab}[\gamma_b+in''Kv]^{-1} \end{aligned} \tag{8.4b}$$

are complex Lorentzians. The fact that $S(y,K)$ contains only odd harmonics and $N(y,K)$ has only even harmonics[5,6] can be seen from the differential equation (2.22) or the integral equation (6.4a), whereby the constant term in $N(y,K)$ couples recursively to produce odd harmonics in the polarization and even harmonics in the populations.

A recursion relation for the d_n alone[10] is obtained by substituting (8.3a) into (8.3b) to give

$$\begin{aligned} d_{n''-2}=&\left(1+\frac{L_{n''+1}^{+}+L_{n''+1}^{-}+8[I\gamma_0^2(M_{n''}^{+}+M_{n''}^{-})]^{-1}}{L_{n''-1}^{+}+L_{n''-1}^{-}}\right)d_{n''} \\ &-\frac{L_{n''+1}^{+}+L_{n''+1}^{-}}{L_{n''-1}^{+}+L_{n''-1}^{-}}d_{n''+2} \end{aligned} \tag{8.5}$$

for $n''\geq 2$ with $d_{-n''}=d_{n''}^*$, and

$$d_0=\{1+\tfrac{1}{2}I\gamma_c(\mathfrak{L}_1^{+}+\mathfrak{L}_1^{-})-\tfrac{1}{2}I\,\mathrm{Re}[(L_1^{+}+L_1^{-})d_2/d_0]\}^{-1}, \tag{8.6}$$

where

$$\mathfrak{L}_1^{\pm}=[\gamma_c^2+(K\pm\delta)^2]^{-1}=|L_1^{\pm}|^2=\tfrac{1}{2}(L_1^{\pm}+L_{-1}^{\mp})/\gamma_c. \tag{8.7}$$

By solving for d_n alone we get faster convergence than solving for d_n and s_n together because we only have to calculate every second coefficient.

The recursion relations (8.3) have previously been solved by using a continued fraction[5-8] which can best be evaluated[9,29] by iterating "convergents" of truncated continued fractions. Recently it has been found[32] in solving the multimode unidirectional traveling-wave laser problem that the continued fraction method is not applicable and recurrence techniques have to be used. It is to be expected that the backward recurrence technique presented here will also prove useful in other related research areas.

The backward recurrence scheme for determining the coefficients $d_{n''}, 0\leq n''\leq n$ (n is some cutoff value), is based on the backward recurrence scheme of Goldstein and Thaler.[37] In this method we first assume that

$$d_{m+2}=0$$

and (8.8)

$$d_m=a,$$

where $m>n$ and a is an arbitrary constant. Substituting this assumption in Eq. (8.5) we recur backward iteratively to obtain all the coefficients $d_{n''}$ for $0\leq n''\leq n$ in terms of a. In general the recursion relation has two solutions but solving only for the $d_{n''}$ with $n''\leq n<m$ assures that we will obtain the solution satisfying the boundary condition $d_{n''}\to 0$ as $n''\to\infty$.[6,37]

The coefficient values thus obtained are not normalized because they depend on our choice of a; however, the ratios between the coefficients approach the exact value as m gets much larger than n. To obtain the normalization for the coefficients we use Eq. (8.6) to determine the value of d_0 from the ratio d_2/d_0. The correct values for all the coefficients are then obtained by using the normalization factor

$$\alpha=\frac{d_0^{\text{normalized}}}{d_0^{\text{unnormalized}}} \tag{8.9}$$

to write

$$d_{n''}^{\text{normalized}}=\alpha d_{n''}^{\text{unnormalized}}. \tag{8.10}$$

Having obtained the $d_{n''}$ coefficients we can get the $s_{n'}$ by using Eq. (8.3a). If we are also interested in evaluating $C(y,K)$ and $M(y,K)$, we write

$$C(y,K)=N_0\sum_{n'=-\infty}^{\infty}{}' c_{n'}e^{in'y}, \quad n' \text{ an odd integer} \tag{8.11a}$$

and

$$M(y,K)=N_0\sum_{n''=-\infty}^{\infty}{}'' m_{n''}e^{in''y},$$

n'' an even integer, (8.11b)

and use the differential equation (2.22) or the integral equation (6.4a) to obtain the relationships

$$c_{n'} = \frac{\delta s_{n'}}{(1+in'K)} \tag{8.12a}$$

and

$$m_{n''} = (M_0/N_0 + \gamma_d)\,\delta_{n'',0} - \gamma_d(1+in''K)^{-1} d_{n''} . \tag{8.12b}$$

The spatially averaged quantities $\vec{\Delta}(K)$ defined in (2.24) are given by

$$\vec{\Delta}(K) = \begin{bmatrix} i(c_1 - c_1^*) \\ i(s_1 - s_1^*) \\ m_0 \\ d_0 \end{bmatrix} = \begin{bmatrix} \delta(I/2)^{1/2}\gamma_0 \,\mathrm{Re}[(L_1^+ + L_1^-)(d_2 - d_0)/(1+iK)] \\ -(2/I)^{1/2}\gamma_0(1-d_0) \\ M_0/N_0 + \gamma_d(1-d_0) \\ d_0 \end{bmatrix} \tag{8.13}$$

Thus if we are interested in $\vec{\Delta}(K)$ we only have to determine d_0 (from the ratio d_2/d_0) and d_2 to obtain all the desired quantities. A listing of the computer program which evaluates $N(K)$ and $S(K)$ using the backward recurrence scheme is given in Appendix F of Ref. 17. The program chooses successively higher cutoff values until the desired accuracy is obtained. The computation time is very fast with about 0.5 sec required to calculate $N(K)$ and $S(K)$ for 100 values of K for about $I = 100$ and increasing slightly for larger I.

In addition to the exact solution discussed above the recursion relations (8.5) and (8.6) can also be used to obtain improved analytic approximations. These are obtained by terminating the Fourier series at successively higher harmonics and solving for coefficients analytically.

For the first approximation we assume that $d_{n''} = 0$ for $n'' \geq 2$, and obtain [from (8.6)]

$$N(K) = N(y,k) = d_0 = [1 + \tfrac{1}{2} I\gamma_c(\mathfrak{L}_1^+ + \mathfrak{L}_1^-)]^{-1} \tag{8.14}$$

which is the rate-equation approximation (REA).[1-6] The next (second recursion relation) approximation is obtained by setting $d_{n''} = 0$ for $n'' \geq 4$. Equation (8.5) then gives

$$d_2/d_0 = (L_1^+ + L_1^-)/\{L_1^+ + L_1^- + L_3^+ + L_3^- + 8[I\gamma_0^2(M_2^+ + M_2^-)]^{-1}\} , \tag{8.15}$$

which substituted in (8.6) results in

$$N(K)/N_0 = d_0 = \left[1 + \tfrac{1}{2} I\gamma_0(\mathfrak{L}_1^+ + \mathfrak{L}_1^-) - \tfrac{1}{2} I\,\mathrm{Re}\left((L_1^+ + L_1^-)^2/\{L_1^+ + L_1^- + L_3^+ + L_3^- + 8[I\gamma_0^2(M_2^+ + M_2^-)]^{-1}\}\right)\right]^{-1} . \tag{8.16}$$

For either approximation [from Eq. (8.13)] we have

$$S(K) = -(2/I)^{1/2}\gamma_0[N_0 - N(K)] \tag{8.17}$$

and a similar equation for S and N integrated over all velocity ensembles [Eq. (2.25)].

The results and discussions presented in the next three sections will show that the second recursion relation approximation (2RCRA) is greatly superior to the REA. Physically it includes coupling effects between the traveling waves which compose the standing-wave field whereas the REA treats them as separate uncoupled waves. This should be especially useful in multimode theory because coupling effects such as mode locking can be obtained using the 2RCRA but not with the REA.

IX. NUMERICAL RESULTS

We will now present the exact numerical results and the analytic approximations to these results obtained by the methods discussed in Sec. III–VIII.

The evaluation of $N(K)$ and $S(K)$ is best accomplished by the backward recurrence scheme (Sec. VIII) or the method of successive continued fraction convergents.[9,29] These methods are about 40 times faster than the direct numerical solution of the differential equation discussed in Sec. VII [requiring about 0.5 sec to evaluate $N(K)$ and $S(K)$ for 100 values of K compared to 20 sec using the differential equation method]. The backward recurrence and successive convergents methods are also valid for arbitrary intensities, detuning, and atomic velocities without experiencing the convergence and roundoff error problems at high intensities (for small velocities and detunings) that manifest themselves with other methods.

Figures 2 and 3 depict the exact numerical results for the spatially averaged population inversion density $N(K)/N_0$ and quadrature polarization coefficient $S(K)/N_0$ for two different intensities and several detunings. A comparison between the exact results, the REA [Eq. (8.14)], and the 2RCRA [Eq. (8.16)] is presented in Figs. 4 and 5. In all cases the graphs are symmetric about the $K = 0$ axis.

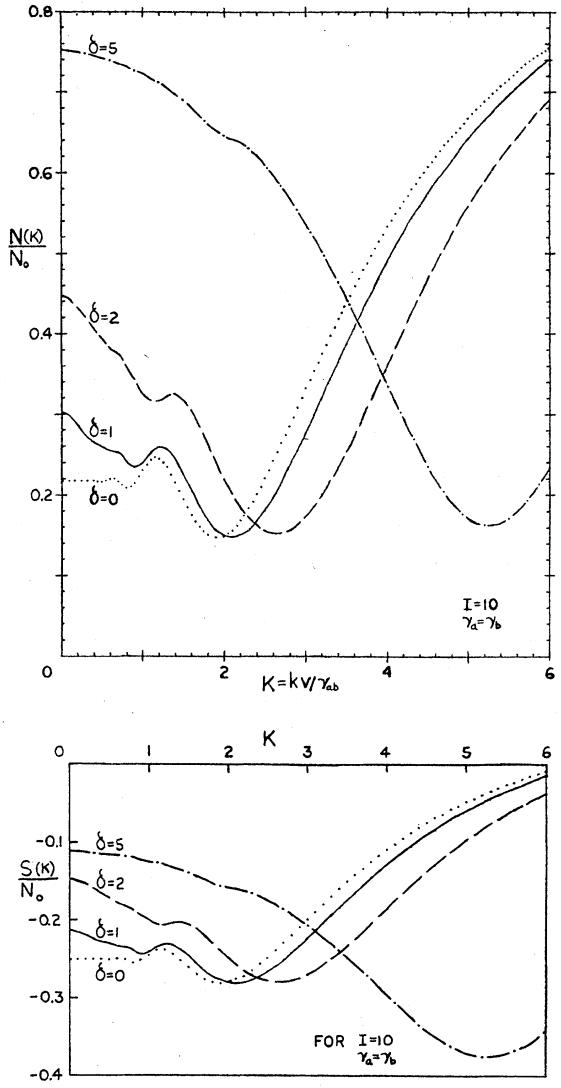

FIG. 2. Graphs of the population inversion density $N(K)$ and quadrature polarization coefficient density $S(K)$ for the general single-mode standing-wave gas laser for an intensity $I=10$ and for several values of the detuning. Note the shift in the position of the major resonance from the $K=\delta$ position and the appearance of the secondary resonances which are especially significant for small detunings.

As seen from Eq. (8.17), the resonance positions in $N(K)$ and $S(K)$ as functions of K coincide. The exact solution shows a shift in the major depletion resonance to the right of the $K=\delta$ position predicted by the REA. This shift is most pronounced for small detunings and increases with high intensities, and can best be interpreted as an AC Stark shift of the atomic transition frequency. The REA treats the problem by considering the standing wave as being composed of uncoupled oppositely

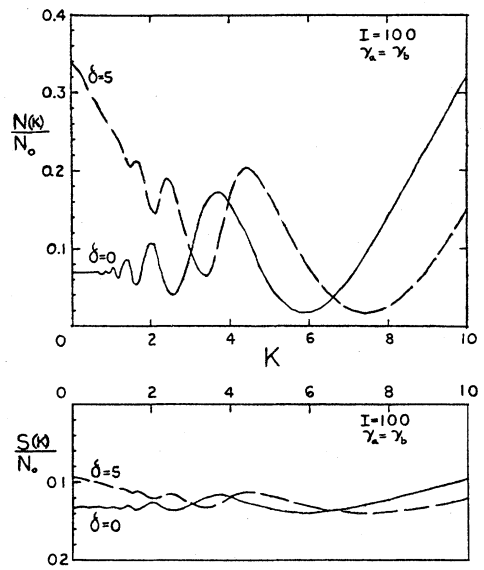

FIG. 3. Graphs of $N(K)$ and $S(K)$ for an intensity of $I=100$ and two detunings. The shift in the position of the major depletion resonance and the appearance of the secondary resonances increases with increased intensity.

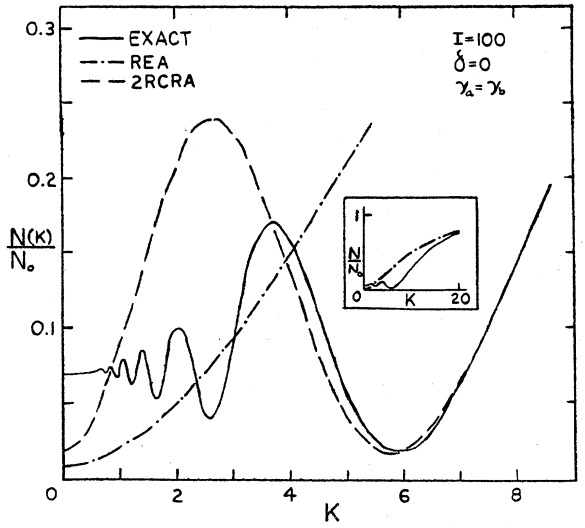

FIG. 4. Comparison of the exact solution for $N(K)$ with the results obtained by the rate-equation (REA) and second recursion relation (2RCRA) approximations. Whereas the REA does not match the exact solution until outside the major resonance (see insert) the 2RCRA matches from the first resonance and outward thus giving the correct shift of the major resonance. The 2RCRA also predicts the existence of one of the secondary resonances.

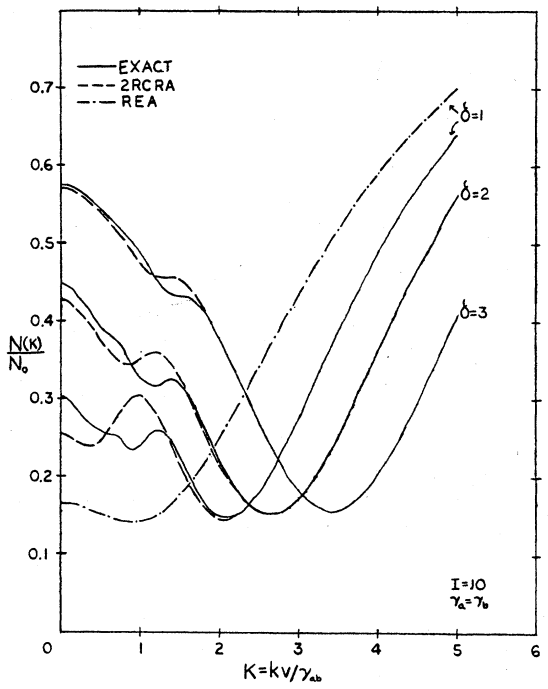

FIG. 5. Comparison between exact, REA, and 2RCRA for $N(K)$ for $I=10$ and several detunings. Again note the greater accuracy of the 2RCRA compared to the REA.

directed traveling waves except insofar as they share, and interact with, the same ensemble of atoms when the detuning is smaller than the atomic linewidth. Thus the REA only predicts a resonance when the Doppler shift and cavity detuning coincide ($K=\pm\delta$), and does not match the exact solution at high intensities except outside the major depletion region. The 2RCRA includes some of the interactive coupling between the two traveling waves thereby exhibiting a Stark-shifted resonance and giving a very close approximation from the position of the first resonance and outward.

Another feature of the exact solution is the appearance of a series of smaller secondary resonances superimposed on the major depletion. These secondary resonances were first predicted by Refs. 5 and 6 for the centrally tuned laser and discussed by Ref. 12 for the saturated absorption problem in terms of two- and three-photon interactions and AC Stark shifts. The number and magnitude of these secondary resonances increases with increased intensity and decreased detuning. The REA which does not include any interactive coupling does not predict any of these secondary resonances. However, the 2RCRA does predict the existence of a secondary resonance. For the case of zero detuning (and equal decay rates and neglecting collision broadening) we have seen in Sec. V that the positions of all the resonances can be obtained from the zeros of the Bessel function $J_0(\chi)$ [Eq. (5.9)]. For general values of the detuning a very good prediction for the resonance positions can be obtained by using a "dressed atom" approach,[36] which treats the atoms as being Stark shifted by part of the field and then considers interactions between these atoms and the remaining field. In Sec. X a physical interpretation of the results in terms of multiphoton interactions and AC Stark shifts will be presented.

X. PHYSICAL INTERPRETATION OF THE RESULTS

To analyze the numerical results presented in Sec. IX we will discuss the interactions between the active atoms and the standing-wave laser field.

For the two-level atom, which is our model for the active medium (Sec. II), the interactions between the atoms and the field can be separated into odd- and even-number photon interactions. The odd-photon processes result in a transition between the two energy levels and the even-photon processes leave the atom in the same energy level. Both types of interactions act to couple the two traveling waves which compose the standing wave.

The simplest type of interaction to discuss is single-photon absorption and stimulated emission. As shown in Fig. 6 the resonance condition for these processes is

$$\tilde{\omega}=\nu\pm kv, \tag{10.1a}$$

i.e.,

$$\tilde{\omega}-\nu=\pm kv \text{ or } \delta=\pm K, \tag{10.1b}$$

where the minus sign is for the traveling wave in the direction of the atom's motion and the plus

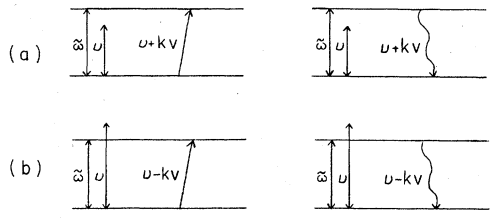

FIG. 6. Illustration of single-photon absorption (upward transition) and stimulated emission (downward transition) with each of the oppositely directed traveling waves which compose the standing wave. The resonance condition for these interactions is $\tilde{\omega}=\nu\pm kv$. (The magnitude of kv is greatly exaggerated with respect to the magnitude of ν and $\tilde{\omega}$ in the illustration for clarity.) (a) Single-photon interactions with wave running antiparallel to the atom's motion (resonance condition: $\tilde{\omega}=\nu+kv$). (b) Single-photon interactions with wave running parallel to the atom's motion (resonance condition: $\tilde{\omega}=\nu-kv$).

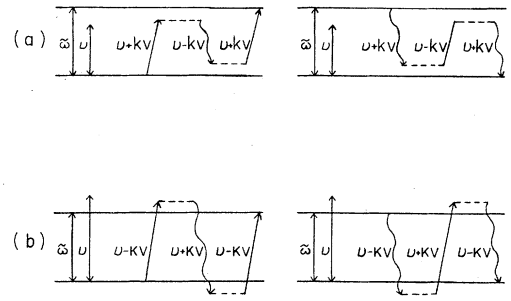

FIG. 7. Illustration of three-photon Raman transitions whereby two photons are absorbed (emitted) from one of the traveling waves and reemitted (reabsorbed) into the other oppositely directed traveling wave. The resonance condition for these interactions is $\tilde{\omega} = \nu + 3kv$. (The magnitude of kv with respect to $\tilde{\omega}$ and ν is greatly exaggerated in the illustration for clarity.) (a) Raman absorption and Raman emission when field frequency ν is smaller than atomic transition frequency $\tilde{\omega}$ [resonance condition: $2(\nu + kv) - (\nu - kv) = \tilde{\omega}$]. (b) Raman absorption and Raman emission when field frequency ν is larger than atomic transition frequency $\tilde{\omega}$ [resonance condition: $2(\nu - kv) - (\nu + kv) = \tilde{\omega}$].

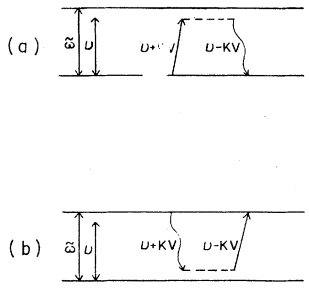

FIG. 8. Illustration of Rayleigh scattering whereby one photon is absorbed (emitted) from one of the traveling waves and another photon is reemitted (reabsorbed) into the oppositely directed traveling wave. The resonance condition for these interactions is $kv = 0$ (again the magnitude of kv is greatly exaggerated for clarity). (a) Two-photon Rayleigh scattering with atom in the lower state b (resonance condition: $\nu + kv = \nu - kv$). (b) Two-photon Rayleigh scattering with atom in upper state a (resonance condition: $\nu + kv = \nu - kv$).

sign for the oppositely directed traveling wave.

The other odd-multiphoton processes can be illustrated by the three-photon Raman transition. As shown in Fig. 7 this results when the atom absorbs (emits) two photons from one of the traveling waves and reemits (reabsorbs) one photon into the opposite traveling wave. These interactions thus lead to a coupling between the two traveling waves. The resonance condition for the Raman transition is

$$\tilde{\omega} = 2(\nu \pm kv) - (\nu \mp kv), \tag{10.2a}$$

i.e.,

$$\tilde{\omega} - \nu = \pm 3kv \text{ or } \delta = \pm 3K, \tag{10.2b}$$

where the plus and minus signs are interpreted as before. The resonance condition for general odd-photon transition interactions, whereby the atom absorbs (emits) n photons from one traveling wave and reemits (reabsorbs) $n-1$ photons into the other traveling wave, is

$$\tilde{\omega} = n(\nu \pm kv) - (n-1)(\nu \mp kv), \tag{10.3a}$$

i.e.,

$$\tilde{\omega} - \nu = \pm(2n-1)kv \text{ or } \delta = \pm(2n-1)K, \tag{10.3b}$$

where $2n-1$ (n a positive integer) is the number of photons involved in the interaction. These interactions give rise to the complex Lorentzians of Eq. (8.4a) which appear in the recursion relations and in the resulting solution with the combination

$$L^{+}_{n'} + L^{-}_{n'} = [\gamma_c + i(\delta + n'K)]^{-1} + [\gamma_c + i(\delta - n'K]^{-1}, \tag{10.4}$$

n' an odd integer.

The sum is due to the fact that the atoms are interacting with both oppositely directed traveling waves.

The even-photon processes are illustrated (Fig. 8) by two-photon Rayleigh scattering. In this interaction one photon is absorbed (emitted) from one traveling wave and another photon reemitted (reabsorbed) into the opposite traveling wave. The resonance condition for the two-photon Rayleigh process is

$$\nu \pm kv = \nu \mp kv \tag{10.6a}$$

or

$$kv = K = 0. \tag{10.6b}$$

For the general even-photon interactions, a number of photons are absorbed (emitted) from one of the traveling waves and an equal number of photons are emitted (absorbed) into the other traveling wave. The atom is thus left in the same state it was before the transition. The resonance condition for the general even-photon interactions is

$$n(\nu \pm kv) = n(\nu \mp kv) \tag{10.7a}$$

or

$$kv = K = 0, \tag{10.7b}$$

where $2n$ is the number of photons involved in the interaction. Thus all the even-photon interactions have their resonances at $K = 0$. These interactions give rise to the Lorentzians of Eq. (8.4b) which appear in the combination

$$M^{+}_{n''} + M^{-}_{n''} = [1+\gamma_d + in''K]^{-1} + [1-\gamma_d + in''K]^{-1}, \quad n'' \text{ an even integer.} \tag{10.8}$$

When only single-photon interactions are considered we obtain the rate-equation approximation (REA). The only coupling between the two traveling waves considered in this approximation is that for small detunings ($\lesssim \tilde{\gamma}_{ab}$) both waves will interact with and share the same set of atoms. For larger detunings each wave will interact with a separate ensemble of atoms related by the resonance condition $K = \pm\delta$ [Eq. (10.1b)]. A distinguishing characteristic of this approximation is the "burning" of depletion resonances or "holes" in the graphs of $N(K)$ vs K at the resonance positions $K = \pm\delta$ (Figs. 4 and 5). For small intensities the REA is a good approximation, but for higher intensities the contributions due to multiphoton interactions have to be considered.

The 2RCRA [Eq. (8.16)] contains Lorentzians describing one-, two-, and three-photon interactions with resonances at $K = \pm\delta, 0, \pm 3\delta$, respectively. The superposition of these three resonances leads to a very good approximation for the first resonance and to the prediction of one secondary resonance (see Figs. 4 and 5).

The superposition of all the odd-number-photon interaction resonances ($K = \pm n'\delta$) and even-number-photon interaction resonances ($K = 0$) results in the structure given by the exact solution. The effects of the superposition become most apparent for the case of central tuning when all the multiphoton (emission and absorption) interactions have their resonances at $K = 0$, but their superposition gives the series of depletion resonances shown in Fig. 4. The appearance of resonances at $K \neq 0$ results from the superposition of emission and absorption resonances (at $K = 0$) of different widths and amplitudes.

The above discussion, however, does not provide a simple means for the prediction of the resonance positions when the superposition becomes important. A related "dressed atom" approach[17,36] does provide an extremely good approximation for the resonance positions. In this approach we consider the atoms as being Stark shifted by the REA field, i.e., a field consisting of two oppositely directed traveling waves which are uncoupled except insofar as they share the same active atoms when the detuning is small. The consideration of multiphoton interactions with these "dressed atoms" that have Stark-shifted transition frequencies leads to a very good prediction for the resonance positions. This approach is presented in more detail in Ref. 36(b). For the case of central tuning we have already discussed the prediction for the resonance positions obtained from the Bessel series solution [Eq. (5.9)].

XI. RELATION BETWEEN EXCITATION, DETUNING, AND INTENSITY

Having analyzed the population inversion density and polarization coefficients as functions of axial position and atomic velocities, we now turn to an analysis of the relationship between pumped excitation N_0, detuning δ, and output intensity I. These relationships are obtained by substituting the macroscopic quadrature polarization coefficient defined by Eq. (2.5) into the amplitude determining Eq. (2.4a) to give

$$(2I\gamma_a\gamma_b)^{1/2}\hbar/\mathcal{P} \equiv E_0 = -Q\mathcal{P}S/\epsilon_0 = -Q\mathcal{P}/\epsilon_0(S/N_0)N_0 \tag{11.1}$$

or

$$N_0 = -(\gamma_{ab}\epsilon_0\hbar/\mathcal{P}^2Q)\gamma_0(2I)^{1/2}(S/N_0)^{-1}, \tag{11.2}$$

where, using (2.25),

$$\frac{S}{N_0} = \int_{-\infty}^{\infty} dK\, W(K)\frac{S(K)}{N_0} = (\overline{K}\sqrt{\pi})^{-1}\int_{-\infty}^{\infty} dK\, e^{-(K/\overline{K})^2}\frac{S(K)}{N_0}. \tag{11.3}$$

It is convenient to express the excitation in terms of the relative excitation ratio

$$\mathfrak{N} \equiv N_0/N_T, \tag{11.4}$$

where N_T is the excitation at threshold, i.e., at the onset of oscillation when the detuning is zero. Thus we write

$$N_T = -\frac{\gamma_{ab}\epsilon_0\hbar}{\mathcal{P}^2Q}\gamma_0\left[\frac{(2I)^{1/2}}{S/N_0}\right]_{I=0,\,\delta=0} \tag{11.5}$$

and

$$\mathfrak{N} = \frac{(2I)^{1/2}/(S/N_0)}{[(2I)^{1/2}/(S/N_0)]_{I=0,\,\delta=0}}. \tag{11.6}$$

Since S/N_0 is a function of the intensity and the detuning, Eq. (11.6) provides a means for relating these quantities to the relative excitation.

The first case we will look at is the stationary-atom laser of Sec. III. In this case all the atoms have zero velocity and hence the integration over velocities in (11.3) is not necessary. Thus we take the exact solution for $S(0)/N_0$ in Eq. (3.6) and substitute in (11.5) to obtain

$$N_T = (\gamma_{ab}\epsilon_0\hbar/\mathcal{P}^2Q)\gamma_c. \tag{11.7}$$

This is the expected result that the threshold excitation is proportional to the losses ($1/Q$) and the collision-broadened linewidth ($\tilde{\gamma}_{ab} = \gamma_{ab}\gamma_c$),

and inversely proportional to the square of the dipole-moment matrix element ($\mathcal{P}^2$). Also from (11.6) we get

$$\mathfrak{N} = \frac{(2I)^{1/2}}{S/N_0}\left(\frac{-\gamma_0}{\gamma_c}\right) = \left(\frac{I}{\gamma_c}\right)[1-(1+2I\gamma_c\mathfrak{L})^{-1/2}]^{-1} \tag{11.8a}$$

or

$$I = \mathfrak{N}\gamma_c - [1+(1+8\mathfrak{N}\gamma_c\mathfrak{L})^{1/2}]/4\mathfrak{L}. \tag{11.8b}$$

These equations relate the detuning, relative excitation, and output intensity in the stationary-atom laser. As discussed by Stenholm and Lamb[5] and implicit in Eqs. (11.8), the intensity is very close to being directly proportional to the excitation.

Experimentally, absolute values of the relative excitation are difficult to measure because the excitation level achieved in the laser medium is not a simple function of the pump energy. Thus for comparison to experiments it is useful to obtain a "detuning curve" which gives the output intensity as a function of the detuning for fixed excitation values. The detuning curve in Fig. 9 was obtained by using Eq. (11.8b). It has a characteristic Lorentzian shape with a maximum intensity at zero detuning and a sharply decreasing intensity as the detuning increases until it reaches zero when the detuning is too large to sustain oscillations at the given excitation.

For the case of moving atoms, the threshold excitation can be obtained by using the rate equation approximation because the REA is essentially exact for small intensities. Substituting the REA value for $S(K)/N_0$ [Eqs (8.14) and (8.17)] into (11.3), we have

$$\frac{S}{N_0} = (\bar{K}\sqrt{\pi})^{-1}\int_{-\infty}^{\infty} dK\, e^{-(K/\bar{K})^2}[-(I/2)^{1/2}\gamma_0\gamma_c(\mathfrak{L}_1^+ + \mathfrak{L}_1^-)] \times[1+\tfrac{1}{2}I\gamma_c(\mathfrak{L}_1^+ + \mathfrak{L}_1^-)]^{-1} \tag{11.9a}$$

$$= \frac{-(2I)^{1/2}\gamma_0\gamma_c}{\bar{K}\sqrt{\pi}}\int_{-\infty}^{\infty} dK\, e^{-(K/\bar{K})^2} \times\mathfrak{L}_1^+[1+\tfrac{1}{2}I\gamma_c(\mathfrak{L}_1^+ + \mathfrak{L}_1^-)]^{-1}, \tag{11.9b}$$

which, when substituted in (11.5), gives

$$N_T = \frac{\gamma_{ab}\epsilon_0\hbar}{\mathcal{P}^2 Q}\frac{\bar{K}\sqrt{\pi}}{\gamma_c}\left[\int_{-\infty}^{\infty} dK\, e^{-(K/\bar{K})^2}(\gamma_c^2+K^2)^{-1}\right]^{-1}. \tag{11.10}$$

Using Ref. 25, Eq. (3.4666-1) we get

$$N_T = (\gamma_{ab}\epsilon_0\hbar/\mathcal{P}^2 Q)(\bar{K}/\sqrt{\pi})e^{-(\gamma_c/\bar{K})^2}[1-\Phi(\gamma_c/\bar{K})], \tag{11.11}$$

where the error function Φ is defined by [Ref. 21, (Eq. 8.250-1)]

$$\Phi(\gamma_c/\bar{K}) = 2\pi^{-1/2}\int_0^{\gamma_c/\bar{K}} dt e^{-t^2} = \sum_{l=0}^{\infty}(-1)^l(\gamma_c/\bar{K})^{2l+1}[l!(2l+1)]^{-1}. \tag{11.12}$$

This result is equivalent to the result obtained by Lamb[1] [Eq. (60)] using the perturbation solution if we note that the imaginary part of the plasma dispersion function is

$$Z_i(0+i/\bar{K}) = \sqrt{\pi}\,[1-\Phi(1/\bar{K})]e^{1/\bar{K}^2}. \tag{11.13}$$

Comparing (11.11) to the threshold excitation for the stationary-atom laser, Eq. (11.7), one finds that whereas for stationary atoms N_T is proportional to the collision-broadened homogeneous linewidth $\tilde{\gamma}_{ab} = \gamma_{ab}\gamma_c$, for moving atoms N_T is proportional to the Doppler broadening $ku = \gamma_{ab}\bar{K}$ and to a factor which depends on the homogeneous to inhomogeneous linewidth ratio $\tilde{\gamma}_{ab}/ku = \gamma_c/\bar{K}$.

The relative excitation $\mathfrak{N}$ is obtained by substituting (11.11) into (11.4) to get

$$\mathfrak{N} = -(\gamma_0\pi^{1/2}/\bar{K})[1-\Phi(\gamma_c/\bar{K})]e^{(\gamma_c/\bar{K})^2}\frac{(2I)^{1/2}}{S/N_0}. \tag{11.14}$$

This provides a relationship between the relative excitation $\mathfrak{N}$, intensity I, and detuning δ, when we substitute a solution for S/N_0. This solution could be the velocity integral over any of the exact or approximate solutions for $S(K)/N_0$ which were discussed in previous sections. Because the velocity

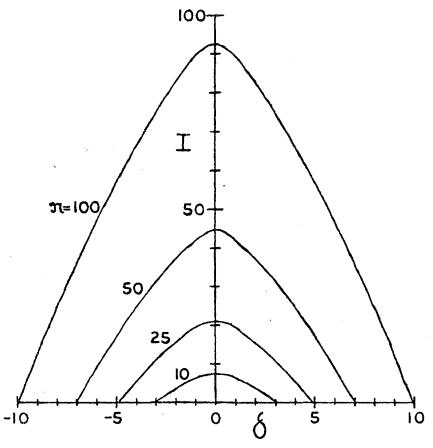

FIG. 9. Detuning curves for the stationary-atom laser showing the variation of the intensity as a function of the detuning. Note the Lorentzian shape with a maximum at $\delta = 0$.

integral of the solutions for moving atoms, even of the analytic approximations, can be done exactly only by numerical methods, Eq. (11.14) cannot be solved analytically for I as a function of δ and $\mathfrak{N}$ as was possible for the stationary-atom laser [Eq. (11.8b)]. We thus cannot directly obtain a "detuning curve" for the moving-atom laser. Such curves are obtained by indirect means as discussed below.

Stenholm and Lamb[5] have described a graphical method for obtaining a detuning curve. In this method several graphs are first drawn using Eq. (11.14) to graph the relative excitation as a function of the intensity for several values of the detuning. By drawing a straight line through the graphs at the desired value of $\mathfrak{N}$ we can read off the value of I at each value of the detuning for which a curve has been drawn. The values of I as a function of δ for the fixed $\mathfrak{N}$ are then used to draw the detuning curve. This method, however, can be inaccurate and time consuming because the accuracy depends on how many graphs are drawn and how accurately they are read, and the computation of many extra values of $\mathfrak{N}(\delta,I)$ are required than are actually used to draw the detuning curve.

The method we have used to obtain detuning curves for the moving-atom laser is to calculate $\mathfrak{N}(\delta,I)$ for several values about the desired $\mathfrak{N}$. Starting with a given detuning (e.g., $\delta=0$) and choosing an appropriate starting value for the intensity I we calculate $\mathfrak{N}(\delta,I)$. Then increasing or decreasing I depending on whether the calculated $\mathfrak{N}$ is lower or higher, respectively, than the desired $\mathfrak{N}$, we calculate a new $\mathfrak{N}(\delta,I)$. This process is repeated until the desired $\mathfrak{N}$ is between two calculated values of $\mathfrak{N}$. The results are then interpolated to obtain the I associated with the desired $\mathfrak{N}$ at the given δ. By increasing δ incrementally and repeating the process using the last value of I as the appropriate starting value for the intensity, we obtain a series of (δ,I) pairs associated with the desired $\mathfrak{N}$. These pairs are then used to draw the detuning curve.

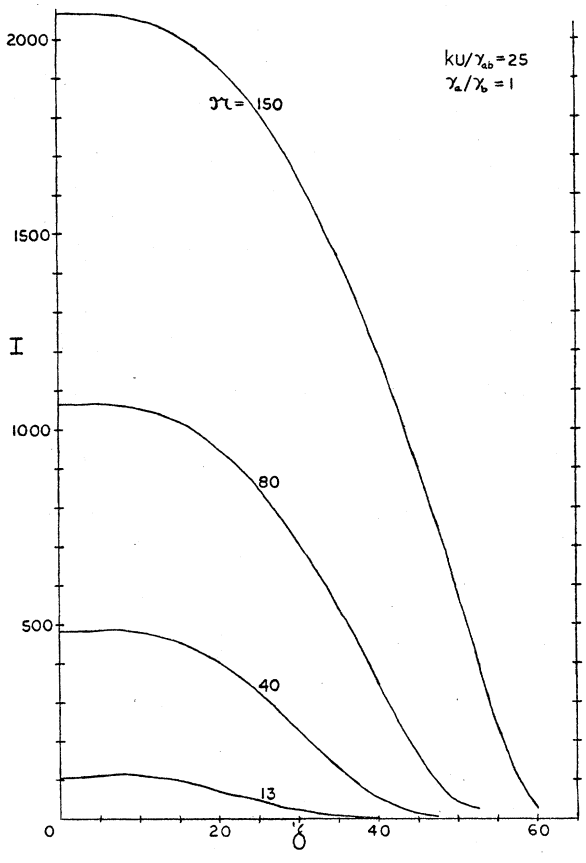

FIG. 10. Detuning curves for the moving-atom laser with a Doppler width of $ku/\gamma_{ab}=25$ for several relative excitations $\mathfrak{N}$. Note the decrease and disappearance of the Lamb dip as the excitation increases.

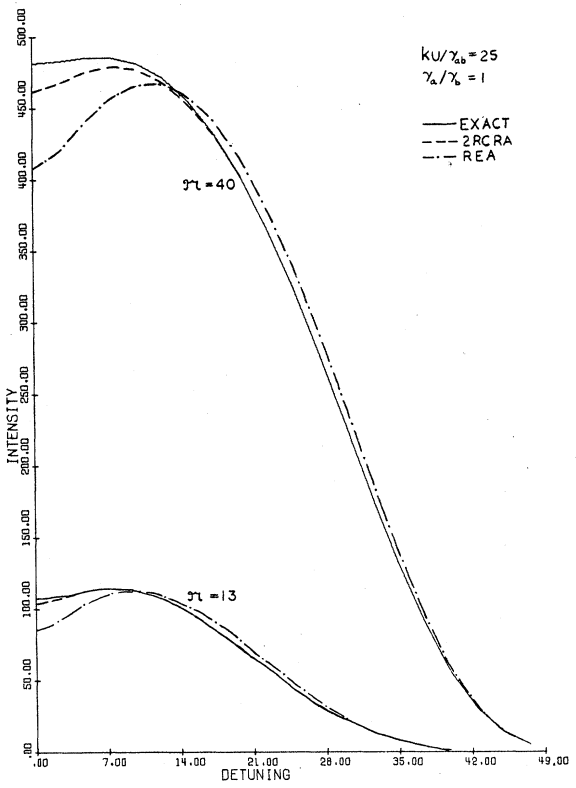

FIG. 11. Comparison between the exact detuning curve and those obtained by the REA and 2RCRA. Whereas the REA does not match the exact solution except at the wings, the 2RCRA matches the exact curve except at small detunings. Both of these approximations do not show the decrease in the depth of the Lamb dip with increased excitation which appears in the exact curve.

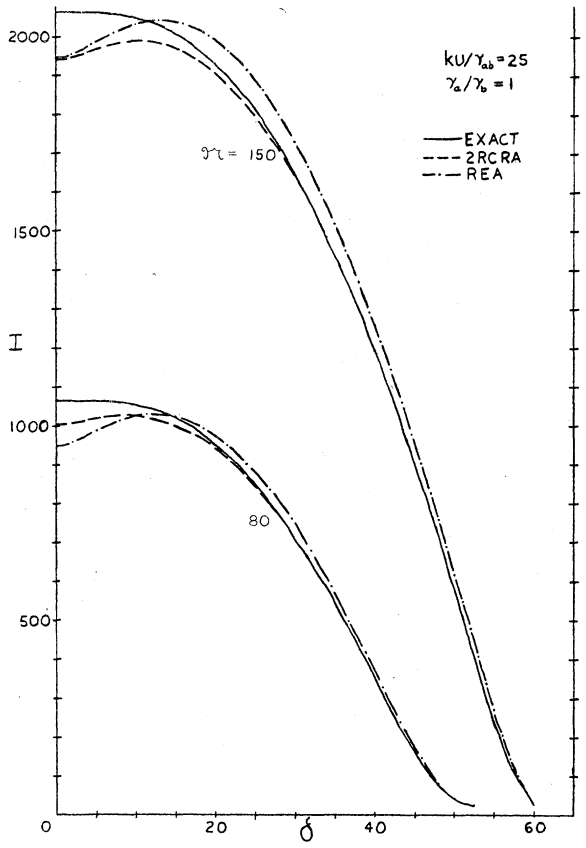

FIG. 12. Comparison between the exact, REA, and 2RCRA detuning curves. Note that for $\mathfrak{R} = 150$ the Lamb dip in the REA, although increasing in magnitude, is decreasing as a percentage of the total curve.

The exact detuning curves given in Figs. 10–12 were obtained by using the backward recurrence scheme or the successive convergents continued fraction method (Sec. IX) to obtain exact solutions for $S(K)/N_0$ and then integrating over a Maxwellian velocity distribution using trapezoidal integration to obtain S/N_0. Substituting these values for S/N_0 in Eq. (11.14) gives us values of $\mathfrak{R}(\delta,I)$ which are then interpolated numerically for (δ,I) pairs associated with the desired $\mathfrak{R}$ as discussed above. The time required to calculate each $\mathfrak{R}(\delta,I)$ to an error of $< 10^{-6}$ in $S(K)/N_0$ and integrating over velocities until $S(K)/N_0 < 10^{-6}$ depends on the value of I, δ, and $\overline{K}$ but averaged about 0.8 sec for the values tested. The number of values of $\mathfrak{R}(\delta,I)$ that have to be calculated in order to be able to interpolate the (δ,I) pair associated with the desired $\mathfrak{R}$ depends on the stepsize in δ and I, and on the slope of the detuning curve at the δ being calculated. The REA and 2RCRA detuning curves are obtained by using the same integration and interpolation method except that the analytic expressions for $S(K)/N_0$ given by these approximations are used to obtain the values of S/N_0.

One of the outstanding features of the standing-wave gas-laser detuning curves is the existence of the Lamb dip,[1] i.e., the increase in intensity as the detuning is increased. The appearance of the Lamb dip is related to the standing-wave character of the field and the inhomogeneous Doppler-broadened linewidths of the moving atoms. The dip does not appear in the stationary-atom standing-wave laser (see Fig. 9) because all the atoms have their resonance at zero detuning. The dip also does not appear in a unidirectional traveling-wave laser even with moving atoms. For such a laser if we assume a flat velocity distribution, then the intensity at a given excitation will be the same for all values of the detuning. This is because at each value of the detuning there will be the same number of atoms with the resonant $K = \delta$ velocity to support the field. For a Maxwellian distribution the maximum intensity will result when $\delta = 0$ because there are more atoms at $K = 0$ to support the field than at any other velocity.

In the standing-wave moving-atom laser with a flat velocity distribution the intensity increases as the detuning is increased—approaching an asymptotic value as $\delta \to \infty$.[7] This is related to the fact that as the detuning increases the velocity of the atoms which interact resonantly increases and they begin to interact resonantly with only one of the traveling waves which compose the standing wave, i.e., with only part of the total field. These faster-moving velocity ensembles are thus saturated by only a part of the field and therefore can support a larger total field than slower-velocity ensembles with the same number of atoms which are saturated by the entire field. Thus for a flat velocity distribution, graphs of the population inversion density as a function of atomic velocity, $N(K)$, would show that the area of the two "holes" burned at $K = \pm\delta$ always increases as δ increases; i.e., the number of atoms supporting the field increases with larger detuning and is a minimum when the two holes merge into a single hole at $\delta = 0$. Consequently the detuning curve for a flat velocity distribution shows a minimum intensity at $\delta = 0$. (In the REA the intensity at $\delta = 0$ is one half the asymptotic value as $\delta \to \infty$.[3]) For a Maxwellian distribution, with a reduced number of available atoms in the faster-moving ensembles, as the detuning increases the intensity first increases as for a flat distribution and then decreases because of the reduced number of atoms resulting in the Lamb dip (Figs. 10–12). Graphs of the population inversion density (Figs. 2–5) show that the area of the holes increases and then decreases as δ is increased.

Secondary resonances such as those which appear in graphs of $N(K)$ and $S(K)$ (see Sec. IX) do not manifest themselves in the detuning curves. This is due to the fact that although $S(K)$ has a series of secondary resonances as a function of K, the area under the curve (integral over K) always increases as a function of δ for a flat velocity distribution. For a Maxwellian distribution the area increases and than decreases as discussed above producing a single Lamb dip.

Although there is always a dip in the detuning curve for an infinite flat velocity distribution, for a Maxwellian distribution the Lamb dip does not appear until[1]

$$\mathfrak{A} > (1 - 2/\overline{K})^{-1}. \qquad (11.15)$$

It does not appear at smaller $\mathfrak{A}$ because the Maxwellian (by reducing the number of available atoms) suppresses the increase in intensity which would appear for a flat velocity distribution. As the excitation is increased the depth of the Lamb dip increases.[5,7] However for large excitations, as shown in Figs. 10 and 11, the depth of the Lamb dip starts decreasing as the excitation increases until it disappears. This decrease and disappearance of the Lamb dip for very high intensities was predicted by Greenstein[3] using the REA. This decrease occurs because as the intensity increases the essentially homogeneous power-broadening increases. When the power broadening becomes comparable to the inhomogeneous Doppler broadening, then all the available velocity ensembles begin to interact with and are saturated by both oppositely directed traveling waves. The saturation of the population inversion thus begins to resemble the saturation in the stationary-atom laser which results in a maximum intensity at zero detuning and a continually decreasing intensity as the detuning increases. This is apparent in Fig. 10 where the detuning curve changes from a Gaussian to Lorentzian shape as the excitation increases (compare to Fig. 9).

Figures 11 and 12 compare the detuning curves obtained by the exact solution (continued fraction or backward recurrence), the REA, and the 2RCRA. It is apparent that the 2RCRA is a much better approximation than the REA—converging rapidly to the exact solution whereas the REA is close but does not converge to the exact solution for higher intensities except near the wings of the detuning curve. Both of these approximations do not show the decrease and disappeareance of the Lamb dip in the region $(1 < \mathfrak{A} < 300)$ that was tested. These approximations showed the Lamb dip always getting deeper as the excitation increases. However the depth of the Lamb dip divided by the intensity at $\delta = 0$ (fractional depth) decreases in the REA as the excitation increases, and in the 2RCRA the fractional depth decreases until about $\mathfrak{A} = 150$ and then increases. Although Greenstein[3] predicted the decrease and disappearance of the Lamb dip by using the REA in the limit of $I \to \infty$ his quantitative prediction for when this occurs ($\mathfrak{A} = 1.7$) is based on a strongly inhomogeneous approximation to the REA and thus does not match the numerical results depicted in the graphs (Figs. 11 and 12).

XII. SUMMARY

This research has resulted in the development of new mathematical methods for the study of the high-intensity gas laser. These methods have been used to obtain exact numerical solutions, analytic approximations, and in special cases exact analytic solutions. In addition we have obtained some new physical results and presented new physical interpretations for some of the previously well-known results.

The fastest and most accurate methods for obtaining exact numerical results for the population inversion and polarization densities is to solve the recursion relations for the coefficients in a Fourier series solution by using the backward recurrence scheme or the successive convergents method for evaluating the continued fraction solution (Sec. VIII) to the recursion relations.

The laser equations were also formulated as a matrix differential equation with periodic boundary conditions and then solved by various additional methods. These include using numerical methods to convert the periodic boundary conditions to initial conditions and then solving the resulting initial-value problem (Sec. VII). Also directly integrating the matrix differential equation leads to integral equations for the general single-mode laser and to a definite integral which can be integrated analytically in terms of Bessel functions for the special case of zero detuning, equal decay rates, and neglecting collision broadening (Secs. IV–VI).

One of the Bessel function solutions also provides a prediction for the occurence of the secondary resonances in $N(K)$ at the zeros of $J_0[(2I)^{1/2}/K]$.

Terminating the Fourier series and solving for the remaining coefficients analytically gives the best analytic approximations, the REA and 2RCRA, to the solution (Sec. VIII). The 2RCRA, in particular, is a very good approximation—matching the exact solution for $N(K)$ and $S(K)$ from the first secondary resonance and outward and matching the exact detuning curve except at small detunings.

One of the physical results obtained by the exact solution is the decrease and disappearance

of the Lamb dip at high intensities which was first predicted by Greenstein.[3] The depth starts decreasing for intensities above $I = 600$ for a Maxwellian distribution with $ku/\gamma_{ab} = 25$. These intensities are not unusual in present day lasers since (for typical decay rates of 10 MHz and dipole moment of 10^{-29} cm) the power output in a 1-mm-diam beam is about $10^{-4}I$ W [$I = 10^{-2} \times$ power density/(W/m^2)]. This decrease in the Lamb dip occurs when the homogeneous power broadening becomes comparable to the inhomogeneous Doppler broadening. When this occurs the detuning curve also begins to take on a Lorentzian rather than a Maxwellian shape (Sec. XI). This should have important implications in the Lamb dip stabilization of lasers by noting that the maximum stability can be achieved at intermediate intensity levels.

The physical interpretation of the resonances in $S(K)$ and $N(K)$ includes a discussion of multiphoton interactions between the atoms and the field. These interactions include odd-number-photon transitions such as single-photon absorption and emission and three-photon Raman transitions, and the even-number-photon scattering interactions such as two-photon Rayleigh scattering (Sec. X).

The mathematical methods presented in this research should also be useful in related areas of multimode[39] and ring laser theory and saturated absorption spectroscopy. The stationary-atom multimode laser is mathematically equivalent to the steady state single-mode moving-atom laser except that instead of spatial harmonics we have temporal harmonics. The physical results however will be different since they will include mode competition, frequency pulling, etc.

---

*Work supported by the U.S. Army Research Office.

†This paper is based in part on material submitted by J. Ziegler in partial fulfillment of the requirements for the degree of Doctor of Philosophy at New York University. Supported in part by NSF Traineeship, NDEA Title IV Fellowship, and U.S. Army Research Office. Present address: ITT Avionics Div., 390 Washington Ave., Nutley, N.J. 07110.

[1]W. E. Lamb, Jr., Phys. Rev. 134, A1429 (1964).
[2]W. R. Bennett, Jr., Appl. Opt. Suppl. 1, 24–61 (1962).
[3]H. Greenstein, Phys. Rev. 175, 438 (1968).
[4]N. L. Balazs and I. Tobias, Philos. Trans. R. Soc. Lond. 264, 1 (1969).
[5]S. Stenholm and W. E. Lamb, Jr., Phys. Rev. 181, 618 (1969).
[6]B. J. Feldman and M. S. Feld, Phys. Rev. A 1, 1375 (1970).
[7]H. K. Holt, Phys. Rev. A 2, 233 (1970).
[8]K. Kuroda and I. Ogura, J. Appl. Phys. Jpn. 12, 1758 (1973).
[9]B. J. Feldman and M. S. Feld, Phys. Rev. A 5, 899 (1972).
[10]L. N. Menegozzi and W. E. Lamb, Jr., Phys. Rev. A 8, 2103 (1973).
[11]M. Salomaa and R. Salomaa, Physica Fennica 8, 289 (1973).
[12]S. Haroche and F. Hartmann, Phys. Rev. A 6, 1280 (1972).
[13]J. H. Shirley, Phys. Rev. A 8, 347 (1973).
[14]S. G. Rautian and I. I. Sobelman, Zh. Eksp. Teor. Fiz. 44, 934 (1963) [Sov. Phys.-JETP 17, 635 (1973)].
[15]S. Stenholm, Phys. Rev. B 1, 15 (1970).
[16]K. Uehara and K. Shimoda (unpublished).
[17]J. Ziegler, Ph.D. thesis (New York University, 1975).
[18]P. R. Berman and W. E. Lamb, Jr., Phys. Rev. A 2, 2453 (1970); A 4, 319 (1971); P. R. Berman, J. Quant. Spectrosc. Radiat. Transfer 12, 1331 (1972); Appl. Phys. 6, 283 (1975).
[19]F. M. Arscott, *Periodic Differential Equations* (Macmillan, New York, 1964).
[20]A. E. Siegman, *An Introduction to Lasers and Masers* (McGraw-Hill, New York, 1971), Chaps. 3 and 9.
[21]I. S. Gradshteyn and I. M. Ryzhik, *Table of Integrals, Series, and Products* (Academic, New York, 1965).
[22]*Handbook of Mathematical Functions*, edited by M. Abramowitz and I. A. Stegun (Dover, New York, 1965).
[23]E. A. Coddington and N. Levinson, *Theory of Ordinary Differential Equations* (McGraw-Hill, New York, 1955), Chap. 2 and especially p. 76.
[24]R. Bronson, *Matrix Methods, An Introduction* (Academic, New York, 1969), Chaps. 6 and 7.
[25]W. E. Boyce and R. C. DiPrima, *Elementary Differential Equations and Boundary Value Problems* (Wiley, New York, 1969), Chap. 7; F. Brauer and J. A. Nohel, *Qualitative Theory of Ordinary Differential Equations*, (Benjamin, New York, 1969), Chap. 2.
[26]W. V. Lovitt, *Linear Integral Equations* (McGraw-Hill, New York, 1924), Chap. II; J. Mathews and R. L. Walker, *Mathematical Methods of Physics* (Benjamin, New York, 1965), Chap. 11.
[27]J. S. R. Chisholm, in *The Padé Approximant in Theoretical Physics*, edited by G. A. Baker, Jr., and J. L. Gammel (Academic, New York, 1970), Chap. 5.
[28]G. A. Baker, Jr., *Essentials of Padé Approximants* (Academic, New York, 1975).
[29]G. N. Lance, *Numerical Methods for High Speed Computers*, (Iliffe, London, 1960), Chap. 3.
[30]T. R. Goodman and G. N. Lance, Math. Tables and Aids to Comp. 10, 82 (1956).
[31]Y. L. Luke, *The Special Functions and Their Approximations*, Vol. II (Academic, New York, 1965), Sec. 12.5.
[32]J. B. Hambenne and M. Sargent, III, Phys. Rev. A 13, 784 (1976); A 13, 797 (1976).
[33]P. M. DeRusso, R. J. Roy, and C. M. Close, *State Variables for Engineers* (Wiley, New York, 1965), Chap. 4; A. Messiah, *Quantum Mechanics* (Wiley, New York, 1958), p. 442.

[34]G. N. Watson, *A Treatise on the Theory of Bessel Functions*, 2nd ed. (Cambridge U.P., Cambridge, 1966).

[35]J. D. Jackson, *Classical Electrodynamics* (Wiley, New York, 1962), p. 72.

[36](a) P. R. Berman and J. Ziegler, Bull. Am. Phys. Soc. 20, 636 (1975); *Laser Spectroscopy*, edited by S. Haroche, J. C. Pebay-Peyroula, T. W. Hänsch, and S. E. Harris (Springer-Verlag, Berlin, 1975), p. 464. (b) P. R. Berman and J. Ziegler, Phys. Rev. A 15, 2042 (1977).

[37]M. Goldstein and R. M. Thaler, Math. Tables and Aids to Comp. 12, 18 (1958); *ibid.* 13, 102 (1959).

[38]It can also be obtained directly from the differential equations by substituting a Fourier series for C, S, M, N, and then eliminating C and M by substituting to get a recursion between S and N only.

[39]*Note added in proof:* A recent paper, A. Bambini, Phys. Rev. A 14, 1479 (1976), uses an integral equation solution to study multimode laser operation and obtain solutions for several special cases.